University of Alberta

A Study on Plasma-based Surface Modification and Patterning

by

Jinan Chai

A thesis submitted to the Faculty of Graduate Studies and Research in partial fulfillment of the requirements for the degree of Master of Science.

Department of Mechanical Engineering

Edmonton, Alberta

Fall 2004

Your file Votre référence
ISBN: 0-612-95718-7
Our file Notre référence
ISBN: 0-612-95718-7

" The most beautiful experience we can have is the mysterious. It is the fundamental emotion which stands at the cradle of true art and true science."

–Albert Einstein

To the memory of my late mother

ACKNOWLEDGEMENTS

First and foremost, I would like to thank my advisor, Professor Daniel Y. Kwok, for giving me the opportunity to work in the Nanoscale Technology and Engineering Lab. in this exciting research field. I sincerely appreciate his patient guidance, continual support and helpful suggestions during the past two years.

I would like to acknowledge visiting scholar Dr. Baoming Li, for his initially helping to get me involved into the plasma processing project.

I am grateful to my lab mates, colleagues and friends for my questions and interruptions of their work. Thanks to all my lab mates for creating a rich and delightful research environment in our lab.

I would like to express my gratitude to my thesis committee, Professor Walied Moussa and Professor Krishnaswamy Nandakumar, for reading my thesis and providing comments within a limited amount of time.

I would express my thanks to Nanofab and Alberta Centre for Surface Engineering and Science, where I was provided with the access to the advanced metrological facilities including XPS, SEM and profilometer.

Special thanks to all the machinists and technicians: Albert Yeun, Terri Nord, Dirk Kelm, Rick Bubenko, Bernie Faulkner, Dave Pape and Ian Buttar whose knowledge and abilities helped me a great deal.

I gratefully acknowledge funding for my research by Alberta Ingenuity

Scholarship.

Finally, I would like to thank my grandparents, my father, my aunt and my wife, for their love and consistent care. Particularly, this dissertation is dedicated to my mother, Yidi Guo, who instilled in me the love and importance of education and for whom I owe an enormous debt of gratitude.

Contents

List of Tables

List of Figures

NOMENCLATURE

ADSA-P	axisymmetric drop shape analysis-profile
CASING	crosslinking via activated species of inert gases
CVD	chemical vapor deposition
EDL	electric double layer
ESCA	electron spectroscopy for chemical analysis
MHCD	micro hollow cathode discharge
MSE	micro structure electrodes
PE-CVD	plasma-enhanced chemical vapor deposition
PMMA	polymethyl methacrylate
SAMs	self-assembled monolayers
SEM	scanning electron microscopy

sccm ..... standard cubic centimeters per minute

VUV ..... vacuum ultraviolet

XPS ..... X-ray photoelectron spectroscopy

$CH_3(CH_2)_{17}SH$ ..... Octadecanethiol

$HS(CH_2)_{15}COOH$ ..... 16-mercaptohexadecanoic acid

CHAPTER 1

INTRODUCTION

1.1 Motivations

The past two decades have witnessed a tremendous surge in interest regarding various techniques for material surface preparation and modification. Among these techniques, plasma-based methods are extremely attractive in material processing for surface modification since they make it possible to change the surface properties of a material without changing its bulk properties. This essentially creates "new" materials with new possibilities, opening novel perspectives to help resolve production or design issues and develop innovative applications. Nonequilibrium plasma processing offers distinct advantages over alternate techniques including the modification of just the outermost atomic layers of a substrate, selection of desired chemical reaction pathways, minimization of thermal degradation, rapid treatment and eliminating the waste disposal issues due to its "dry" process.

While plasma is widely used in etching and deposition of semiconductor, dielectric and metallic materials in microelectronics manufacturing, plasma processing of polymeric materials is also being explored in industries and academia in recent years.

Because of their attractive thermal, mechanical and electrical properties, polymers are important to a number of technological fields, including the biomedical, microelectronics, food packaging and printing industries [1, 2]. However, their surface properties often do not meet the demands regarding wettability, biocompatibility and adhesion. For example, polymethyl methacrylate (PMMA) is distinguished by its excellent optical property, high molding precision and cost-effectiveness; its relatively low surface energy may have a negative effect on the adhesion of coating and biocompatibility. Hence, surface modification is required to achieve the desired properties, while maintaining their bulk characteristics [3]. It was shown that substantial changes in the chemical functionality, surface state, wettability, and bondability of polymer surfaces can be achieved by plasma treatment [4, 5, 6, 7].

In spite of successful applications of plasma technique to polymers, precise mechanistic details of processing remain a matter of debate. In order to modify the surfaces of polymeric materials in a well-controlled and reproducible manner, a deeper understanding of plasma-polymer interactions is essential. It is well known that when a polymer is treated with oxidative (oxygen and air) plasma, polar functional groups containing oxygen are introduced into its surface, leading to a hydrophilic surface [8, 9]. However, most work have overlooked the change of electrical properties of plasma treated surfaces and neglected the influence of surface charges on the change in wettability; relatively fewer studies claimed the relationship between surface charge and wettability of the modified surfaces [10]. So far, the cause of wettability change during plasma treatment is not completely understood, the structural state and chemical modification of a surface and its wettability can be complex, and much efforts is

still directed towards understanding the wetting process [11].

In this dissertation, PMMA was selected as a sample polymer substrate to be treated by a DC pulsed oxygen plasma with different times. The changed surface properties including wettability, surface topography and chemical structure were investigated by dynamic contact angle, optical profilometer and X-ray photoelectron spectroscopy (XPS) measurements. The change of surface charge states was also examined by means of zeta potential measurement. The effect of surface charges on the change of wettability was explained from a surface thermodynamic point of view.

In an attempt to further explore the applications of plasma-based surface modification, a micro discharge device was developed for small scale patterning. Self-assembled monolayers (SAMs) were selected as the substrates for microscale modification and Scanning Electron Microscopy (SEM) was employed to image the patterned surface. Due to its ability to produce stable glow discharges at elevated pressure and the ease of manipulation in very small length scale, potential applications of micro discharge plasma in the integrating circuit, biomedical and lab-on-chip communities are desired.

1.2 Thesis Outline

As mentioned earlier, the research work in this thesis contains the studies of surface modification of PMMA in oxygen plasma and possible applications of micro discharge plasma on small scale patterning. The dissertation consists of seven chapters.

Chapter 2 defines plasma in general as well as its main characteristics and classified the types of reactions that can occur in plasma. The mechanisms of interactions taking place between a plasma and a solid surface are also introduced.

Chapter 3 describes the cold plasma generation mechanism, followed by the experimental setup and apparatus of the plasma reactor system. The particular features of DC pulsed discharge are addressed.

Multiple surface analysis tools are presented in Chapter 4. The principles of automated axisymmetric drop shape analysis - profile (ADSA-P) for contact angle measurements and determination of zeta potential are highlighted, followed by the operation principles of X-ray photoelectron spectroscopy (XPS). Furthermore, Optical Profilometer and Scanning Electron Microscopy (SEM) are briefly described.

Chapter 5 details the characterizations of PMMA films after oxygen plasma treatment. XPS, zeta potential and advancing contact angle measurements are employed to investigate the chemical structure, surface charge and wettability. The optical profilometer is used to probe surface morphology. The relationships among the multiple surface properties are discussed and the electrical double layer effect on the change in surface free energy is interpreted.

In Chapter 6, the development of micropatterning process is reported by using a micro discharge device. Alkanethiolates monolayers are prepared by means of self-assembled methods. SEM enables the imaging of patterned surfaces.

Finally, Chapter 7 concludes this thesis with a summary of the results and recommendations for future work.

Chapter 2

Theoretical Background

2.1 Plasma definition and characteristics

Plasmas are ubiquitous, comprising more than 99% of the known matter in the universe. Taking into consideration the energy of the particles constituting the plasma, plasma is energetically the fourth state of materials, which is more highly activated than in the solid, liquid, or a gaseous state. The physics definition of a "plasma" is an ionized gas with an essentially equal density of positive and negative charges. Irving Langmuir and collaborators were the first to study phenomena in plasma in the early 1920's while working on the development of vacuum tubes for large current, and it was Langmuir who in 1929 used the term "plasma" for the first time to describe ionized gases [12]. In a more rigorous way, a plasma can be defined as a quasi-neutral gas of charged and neutral particles characterized by a collective behavior [13].

According to kinetic theory of gases (in an ordinary neutral gas), no forces act between the molecules of the gas (gravitational forces are considered negligible), and the particles travel in straight lines, with a distribution of velocities. The motion of the molecules is controlled by the collision among themselves; hence the molecules

of a neutral gas follow a random Brownian motion. On the contrary, the motion of the particles in a plasma can cause local concentrations of positive and negative electric charges, which can create long-ranged Coulombic fields that affect the motion of charged particles far away from the charge concentrations. Thus, elements of the plasma affect each other, even at large separations, giving the plasma its characteristic collective behavior; hence, a charged particle in a plasma moves along a path which on average follows the electric field.

Local concentrations of charges in a plasma are confined to volumes of small dimensions of size λ_D, where λ_D is a characteristic dimension of the plasma, called the Debye length. The Debye length can be deduced from the Poisson equation and is given by [14]:

$$\lambda_D = (\frac{\varepsilon_0 k T_e}{n_e e^2})^{1/2} \tag{2.1}$$

where ε_0 is the vacuum permittivity, k the Boltzmann constant, e the electron charge, T_e the electron temperature in Kelvin, and n_e the electron density. For a plasma to be stable, it is necessary that the dimensions of the system, L, should be much larger than λ_D. Outside the Debye length (of orders of tens of micrometers), the charge density of ions, which is generally approximately equal to the density of ions n_i, is identical to the density of electrons n_e making the plasma electrically neutral. As a result, plasma is considered a quasi-neutral gas, in which $n_i = n_e = n$, where n is called the plasma density.

The parameter that defines the density of the charged particles in the plasma is the degree of ionization of the gas. It specifies the fraction of the particles in the

gaseous phase which are ionized. The degree of ionization α is defined as

$$\alpha = \frac{n_i}{n_n} \tag{2.2}$$

where n_n is the density of neutrals. For plasmas sustained in low-pressure discharges, the degree of ionization is typically 10^{-6} to 10^{-3}.

Another plasma parameter related to the Debye length is the number of particles N_D in a Debye sphere. It can be taken as

$$N_D = \frac{4\pi}{3} n_e \lambda_D^3 \tag{2.3}$$

The solution of Poisson's equation given by Eq. 2.1 can be obtained only by assuming that the shielding effect is produced by a large number of electrons; in other words, the shielding effect can occur only if the Debye sphere contains a large number of electrons. Thus, N_D has to be much larger than unity to fulfill the collective characteristic of plasma. In cold plasmas, N_D ranges from about 10^4 to 10^7 electrons in a Debye sphere.

Although the plasma bulk is quasi-neutral, local perturbations from neutrality can occur in volumes smaller than the Debye sphere. Due to the low mass of electrons, they will respond faster than the ions to the electric forces generated by the perturbation from neutrality. The response to the perturbation will be through oscillations. The frequency of these electron oscillations is called the plasma or Langmuir frequency ω_p and is given by [15]

$$\omega_p = \left(\frac{n_e e^2}{m_e \varepsilon_0}\right)^{1/2} \tag{2.4}$$

For a typical plasma density of 10^{10} cm^{-3}, the plasma frequency is 9×10^8 Hz. If the charged particles collide too frequently with neutral atoms, their motion is controlled by ordinary hydrodynamic forces rather than by electromagnetic forces. Under these circumstances, the collective behavior condition is not satisfied, and the gas will not behave as a plasma. Hence, if τ is the mean time between collisions of charged particles with neutral atoms, the product $\omega\tau$ has to be bigger than 1 for the gas to behave like a plasma rather than a neutral gas.

Thus it was concluded that, to sustain a plasma in a gas, three conditions have to be met:

$$\lambda_D \ll L \tag{2.5}$$

$$N_D \gg 1 \tag{2.6}$$

$$\omega\tau > 1 \tag{2.7}$$

Plasma is usually generated in electric discharges by transfer of power from an electric field to electrons. In collisions with neutral gas molecules, electrons lose energy to the gas molecules, thus leading to the formation of various reactive particles such as ions, radicals, photons, etc. The different species in the plasma may be characterized by their distinct temperatures. In general, a subdivision can be made between plasmas which are in thermal equilibrium and those which are not in thermal equilibrium. Thermal equilibrium implies that the temperature of all species (electrons, ions, neutral species) is the same. A high gas pressure implies many collisions in the plasma (i.e. a short collision mean free path, compared to the discharge length), leading to an efficient energy exchange between the plasma species, and hence, equal temperatures.

This type of plasma is called hot (or high temperature) plasma. On the other hand, a low gas pressure results in only a few collisions in the plasma (i.e. a long collision mean free path compared to the discharge length), and consequently, different temperatures of the plasma species due to inefficient energy transfer. In this case, the electrons are characterized by much higher temperatures than the heavy particles (ions, atoms, molecules) and this type of plasma is called cold (or low temperature) plasma.

Low pressure plasma, nonequilibrium plasma, and glow discharge are some of the synonymously used terms to designate the same type of process, which is characterized by average electron energies of $1 - 20$ eV and electron densities of $10^8 - 10^{13}$ /cm^3. The plasma in material processing is often referred to as a cold plasma since the absence of thermal equilibrium allows the substrates exposed to the gas remain at a relatively low temperature, while the electrons have sufficient kinetic energy to cause surface modification.

2.2 Collision processes in a plasma

The incessant interchange of energy between the particles of plasmas takes place mainly by collisions, of which we may differentiate between elastic and inelastic collisions. In the former, the particles that have been struck retain the same internal structure, and hence merely acquire greater velocity, while inelastic collisions change the state of the particle itself. The essential mechanisms in the plasma are ionization, excitation, relaxation, dissociation and recombination, which occur mainly as the result of inelastic collisions.

When a primary electron collides with an atom, a portion of the energy ϵ_e carried by the electron is transferred to an electron in the atom or transformed into kinetic energy of the atom. If ϵ_e is relatively small, electrons in the atom remain in the ground state and the collision is an elastic collision. If ϵ_e is greater than the ionization energy of the atom ϵ_i, the atom can be ionized and becomes a positive ion:

$$e + A \rightarrow 2e + A^+ \tag{2.8}$$

To express the frequency of collision, the term cross section is generally used. The probability of ionization, or ionization cross section σ_i, increases with an increase in ϵ_e above ϵ_i, reaches a maximum when ϵ_e is several times greater than ϵ_i, and then decreases with a further increase in ϵ_e, which is explained in that the duration of collision becomes too short for a transfer of energy to an atom as the speed of the electron increases with the energy of the electron.

There are many levels of energy between ground state and ionization energy. If ϵ_{mn} is the energy required to raise a valency electron of an atom from level n to m, and $\epsilon_i > \epsilon_e > \epsilon_{mn}$, an electron within the atom can be lifted to a higher energy level m. This process is known as excitation:

$$e + A \rightarrow e + A^* \tag{2.9}$$

The excited electron usually can stay for a very short period and then returns to a lower energy level or ground state, releasing the gained energy as the emission of a photon:

$$A^* \rightarrow A^* + h\upsilon \tag{2.10}$$

This relaxation process produces a glow discharge. In actual practice, some excited states have much higher stability than others, and such a state is called a metastable state. It can be explained as wider steps on the wall of the potential well [16]. With their long radiative lifetimes, metastables are useful energy-rich chemical reagents. An electron with $\epsilon_e < \epsilon_i$ has no capability of ionizing an atom with ionization energy ϵ_i. However, if the energy level of the metastable atom is ϵ_m and $\epsilon_e + \epsilon_m > \epsilon_i$, ionization of the atom by the low-energy electron becomes possible:

$$e + A^* \rightarrow 2e + A^+ \tag{2.11}$$

An excited atom can also ionize a neutral atom if the excitation energy is larger than the required ionization energy of the latter. This effect is known as the Penning effect [17] and can be an important ionizing agent in gas mixtures since it increases the rates of ionization and excitation:

$$A^* + B \rightarrow A + B^+ + e \tag{2.12}$$

In certain gases, electrons can combine with neutral atoms or molecules to form negative ions. Electronegative gases show this property. In these, the atoms have their outer (almost complete) electron shells and therefore have an affinity for electrons. Important negative ions in gas discharge are F^-, Cl^-, Br^-, I^- and O^-. The most familiar example is oxygen and this process is called attachment:

$$e + O_2 \rightarrow e + 2O \rightarrow O + O^- \tag{2.13}$$

For molecules that consists of atoms, additional levels of internal energy for the

vibration of atoms and rotation of atoms along the axis of a molecule exist. The energy levels for such excitation are generally much lower than the energy levels of the electrons in an atom. Accordingly, a low-energy electron, which cannot excite an atom and causes only elastic collisions with the atom, can yield an inelastic collision with a molecule by transferring the energy to vibrational or rotational levels of internal energy. Therefore, inelastic collisions take place more frequently in molecular gases than in atomic gases, and hence a number of processes may occur when an electron collides with a molecule, including

dissociation:

$$e + A_2 \rightarrow e + 2A \tag{2.14}$$

$$e + AB \rightarrow e + A + B \tag{2.15}$$

dissociative attachment:

$$e + AB \rightarrow A + B^- \tag{2.16}$$

dissociative ionization:

$$e + A_2 \rightarrow e + A^+ + A^- \tag{2.17}$$

$$e + AB \rightarrow e + A^+ + B^- \tag{2.18}$$

For comparison, the dissociation energy, metastable energy and ionization energy for some noble gases and diatomic gases are listed in Table 2.1.

On the other hand, the charged particles are lost from the plasma by recombination of particles of opposite charges due to electrostatic force of attraction. Recom-

binations can take place either between electrons and atomic ions accompanied by radiation or between electrons and molecular ions with dissociation:

$$e + A^+ \rightarrow A + h\nu \tag{2.19}$$

$$e + A_2^+ \rightarrow 2A \tag{2.20}$$

While collisions between electrons and heavy species result in a large number of processes described above, the collisions between heavy species also take place in a plasma and they can be grouped in ion-molecule and molecule-molecule reactions. The effects of ion-molecule collisions are much weaker than those of electron-molecule collisions due to the low speed of ions and the ionization by molecule-molecule collisions is possible only at extremely high temperature. Collisions between charged species causing combinations of positive and negative ions are also considered to be rather small due to the fact that neutral species predominate in a partially ionized gas (nonequilibrium plasma). Hence, inelastic collisions between electrons and heavy species play a key role in plasma assisted surface modification.

2.3 Plasma surface interactions

The modification of physical and chemical structure of a surface which is exposed to a plasma is an extremely complex process. The process results from numerous simultaneous reactions taking place as a consequence of different species produced in the plasma and at the surface of treated material. In general, reactions of gas plasmas with solid surface, especially for polymeric or organic materials, can be classified as follows:

Table 2.1: Dissociation energy, metastable energy and ionization energy for noble and diatomic gases [16]

Gas	Dissociation energy (eV)	Metastable energy (eV)	Ionization energy (eV)
He	-	19.8	24.6
Ne	-	16.6	21.6
Ar	-	11.5	15.8
Kr	-	9.9	14.0
Xe	-	8.32	12.1
H_2	4.5	-	15.6
N_2	9.8	-	15.5
O_2	5.1	-	12.5

1. Etching or ablation
2. Deposition or grafting
3. Crosslinking or branching
4. Activation or functionalization

Each of these effects is always present to some degree, but one may be favored over the others, depending on the substrate, gas chemistry, reactor design, and the operating parameters.

Etching Plasma etching is essentially used to remove material from a surface. The studies of plasma etching of polymers are far less than those for inorganic electronic materials such as silicon and silicon dioxide. However, experimental results have shown that the fundamental etching process for most polymers are similar to that for those inorganic materials. There are basically three different

low pressure plasma etching mechanisms, i.e. (1) physical etching or sputtering, (2) spontaneous chemical etching, and (3) ion-induced chemical etching [18].

In physical sputtering etching, energetic ions accelerated by electric field in a plasma impinge on the surfaces and lose their kinetic energy to the surface. Consequently, the energy loss per impinging ion can break one or more chemical bonds of the atoms or molecules in the substrate, and cause ejection of atoms or molecules for the surface.

In spontaneous chemical etching, reactive neutral or ionized species react with the surface to form volatile products, which depart from the surface spontaneously. For example, this mechanism can be applied for surface preparation and cleaning by breakdown of surface oil and loose contaminants and then removal of volatile products such as CO, CO_2 and H_2O, thereby leaving a uniformly clean and active polymer surface.

Ion-induced chemical etching is a complex process as a result of ion-neutral synergy, in which chemical reaction is only induced or enhanced in presence of energetic ions. Due to the directionality of ion flux, ion-induced chemical etching typically exhibits very high etching rate in a vertical direction while the sidewall of etched structure might experience only minor lateral etching from neutral, leading to a very anisotropic surface.

Deposition In contrast to etching, a process is deposition when the reaction in the gas-phase of plasma or on the surface forms non-volatile products on substrate surface. Plasma deposition process can be subdivided into two groups: sputter-

deposition and plasma-enhanced chemical vapor deposition [19].

Sputter-deposition comprises physical sputtering and reactive sputtering. In physical sputtering, ions (and atoms) from the plasma bombard the target, and release atoms (or molecules) of the target material. The sputtered atoms diffuse through the plasma and arrive at the substrate, where they can be deposited. In reactive sputtering, the dissociation products from a reactive gas will also react with the target. Hence, the film deposited at the substrate will be a combination of sputtered target material and the reactive gas.

Another method of deposition is by plasma-enhanced chemical vapor deposition (PE-CVD). By chemical reactions in the plasma (mainly electron impact ionization and dissociation), different kinds of ions and radicals are formed which diffuse toward the substrate and are deposited by chemical surface reactions. The major advantage of PE-CVD is that it can operate at a much lower temperature. Hence, some coatings which are difficult to form by traditional chemical vapor deposition (CVD) due to melting problems, can be deposited more easily with PE-CVD.

A well-known application of PE-CVD process is plasma polymerization. It refers to the deposition of polymer films through plasma dissociation and to the excitation of an organic monomer gas and subsequent deposition and polymerization of the excited species on the surface of a substrate. The deposited films are called plasma polymers, which are generally chemically and physically different from conventional polymers due to their highly branched and highly

cross-linked properties [13].

Cross-linking CASING (Crosslinking via Activated Species of Inert Gases) was one of the earliest-recognized plasma treatment effects on polymer surfaces [20]. As suggested by the acronym, CASING occurs in polymer surfaces exposed to noble gas plasma (e.g. He or Ar), which are effective at creating free radicals but do not add new chemical functionalities from the gas phase. Ion bombardment or vacuum ultraviolet (VUV) photons can break C−C or C−H bonds, and the free radicals resulting under these conditions can only react with other surface radicals or with other chains in chain-transfer reactions; therefore, they tend to form a very stable surface with crosslinking structure, which may improve the heat resistance and bond strength of the surface by forming a very cohesive skin [5].

It was assumed in the past that crosslinking could be obtained only by using an inert gas, but there are some reports on the crosslinking of polymer even in oxygen plasmas [21]. For example, it was found that the crosslinked skin on propylene (PP) is much thinner than on polyethylene (PE). This is not only because VUV radiation is absorbed in a much thinner layer in PP than in PE, but also because oxygen plasma ablates the polymer at the same time as the crosslinked layer is being formed in the sub-surface region [22].

Activation Surface activation by plasma treatment of a polymer refers to the modification of the properties of its surface by exposure to a nonpolymer forming plasma, such as oxygen, nitrogen and argon. Exposure of polymers to a suitable

plasma can cause chemical and physical changes to their surface or near-surface layers due to interaction (bombardment) with energetic plasma species. As a result, chemical covalent bonds on polymer surfaces break and lead to the formation of surface free radicals. These radicals, in turn, react with the active species of the plasma to form various active chemical functional groups on the surface of the substrate and cause the incorporation of hydrophilic groups, such as carbonyl, carboxyl, hydroxyl and amino groups [23].

By far, oxygen is the most commonly used plasma for chemical surface functionalization and modification. The following oxidation reaction scheme is a logical pathway to produce oxygenated groups grafted on a polymeric surface [9]. First, hydrogen is abstracted from the polymer backbone R by atomic oxygen present in the plasma, leaving the polymer with a free radical site:

$$RH + O \rightarrow R\cdot + \cdot OH \tag{2.21}$$

Then, molecular oxygen can couple with the free radical creating a peroxy radical:

$$R\cdot + O_2 \rightarrow RO_2\cdot \tag{2.22}$$

The peroxy radical can then abstract hydrogen from a neighboring polymer backbone or other source and rearrange into a carboxylic acid groups or an ester:

$$RO_2\cdot + R'H \rightarrow RO_2H + R'\cdot \tag{2.23}$$

$$RO_2\cdot + R'\cdot \rightarrow RO_2R' \tag{2.24}$$

Not indicated in this reaction scheme are the possible formation of alcohols, ethers, peroxides and hydroperoxides. The by products, typically CO_2, H_2O and low molecular weight hydrocarbons, are readily removed by the vacuum pumps.

On the other hand, plasma activation can be used for the opposite conversion of hydrophilic surfaces to hydrophobic surfaces. This can be done with fluorocarbon plasmas, which cause the replacement of surface C−H bonds with C−F bonds or add CF_2 and CF_3 groups to the surfaces of the polymers [24].

Perhaps the most dramatic and widely applied mechanism of plasma treatment is the deliberate alteration of the surface region with new chemical functionalities by activation. Surfaces can thus be engineered to achieve the necessary properties, such as wettabiliy, adhesion, barrier protection, material selectivity, and even biocompatibility [25, 26].

The interaction mechanisms that occur to a solid surface by exposure to a plasma is largely determined by [9]: (1) the process gases, (2) exposure time of the plasma, (3) input energy and power densities, and (4) original composition of the surfaces. Effects of modifications span from relatively simple surface morphological roughening or smooth changes to complex grafting of radically different functional groups or molecular moieties. In spite of the high complexity of the ensuring chemistry in a typical plasma and overlapping of different processes, it is possible to tailor the process to perform specific targeted changes to polymeric surfaces. Figure. 2.1 shows the schematic of collision processes and surface interaction during plasma surface

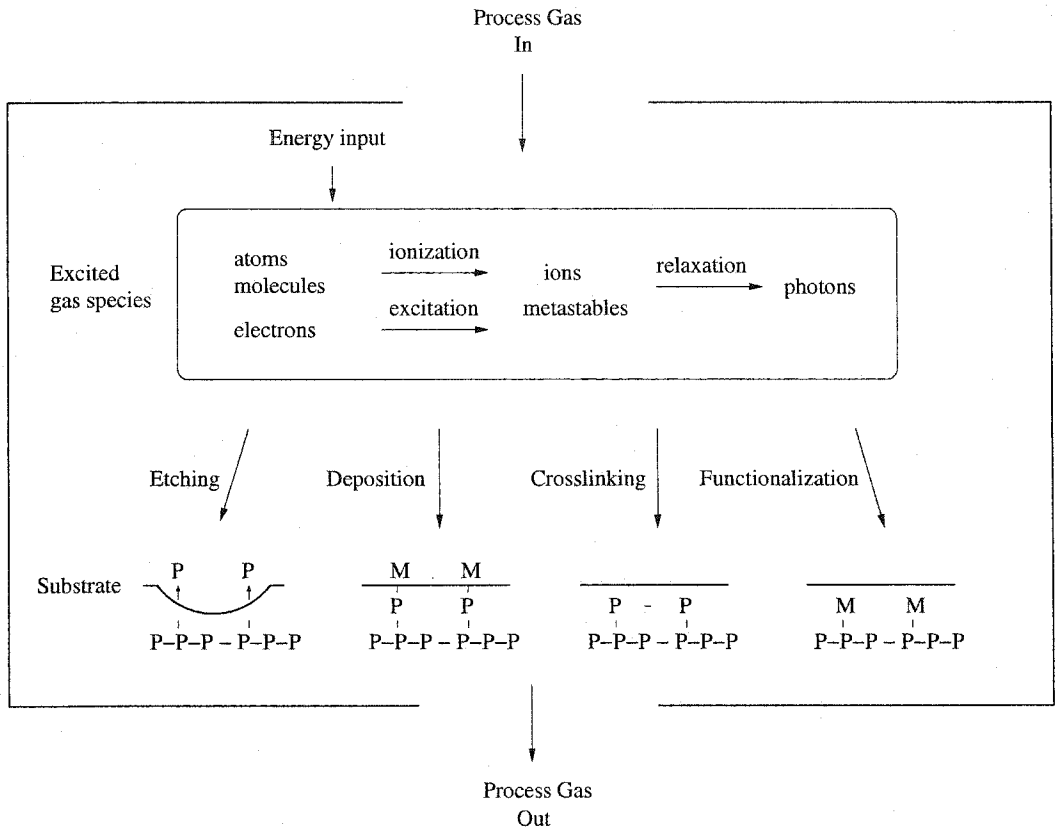

Figure 2.1: Schematic of collision processes and surface interactions during plasma surface modification

modification.

Chapter 3

Experimental Setup and Apparatus

3.1 Cold plasma generation

The most widely used method for plasma generation utilizes the electrical breakdown of a neutral gas in the presence of an external electric field.

Any volume of a neutral gas always contains a small amount of free electrons and ions, as a result of ionization by naturally occurring radioactivity or cosmic rays. As the voltage applied to the electrodes is gradually increased, the available free electrons are accelerated in the electric field, thereby gaining kinetic energy. Concomitantly, the electrons lose energy in collisions with the atoms or molecules of the gas. Large amounts of energy are transferred to those heavy species in the inelastic collisions and the new electrons produced in the ionization process are in turn accelerated by the electric field and produce further ionization by impact with the neutral particles of the gas.

An electron multiplication process thus takes place. This process can be characterized by Townsend's first ionization coefficient α [27], which is defined as the number of ionizing collisions made on the average by an electron as it travels 1 cm

in the direction of the electric field. Considering the increase dn, over a distance dx, in the number of electrons per second crossing a distant x from the cathode, we can obtain

$$dn = \alpha n dx \tag{3.1}$$

$$\int_{n_0}^{n} \frac{dn}{n} = \int_{0}^{x} \alpha dx \tag{3.2}$$

$$n = n_0 \mathrm{e}^{\alpha x} \tag{3.3}$$

where n_0 is the number of electrons per second leaving the cathode. If the electrode spacing is d, then the current can be taken as

$$i = n_0 e \mathrm{e}^{\alpha d} = i_0 \mathrm{e}^{\alpha d} \tag{3.4}$$

where i_0 is the primary current at the cathode and the emitted electrons constituting i_0 are called the primary electrons.

If the mean free path of an electron in the electric field E between all collisions with atoms is λ, then the mean energy gained by an electron between collisions is $Ee\lambda$. α, the number of ionizing collisions made per cm in the field direction, must depend in some way on this energy and at the same time must be proportional to the number of encounters per cm with atoms; the latter condition means that α is proportional to the gas pressure p at constant temperature T. Since it is reasonable to write $\lambda \propto (1/p)$ at constant T, we can get [27]

$$\frac{\alpha}{p} = \phi(\frac{E}{p}) \tag{3.5}$$

where ϕ is some unknown function, which was first derived approximately by Townsend

[28]:

$$\frac{\alpha}{p} = A\mathrm{e}^{-Bp/E} \tag{3.6}$$

in which A and B are constants depending on the gas used.

On the other hand, ions accelerated by the electric field strike the cathode with sufficient energy to cause the emission of secondary electrons from it; the secondary electrons in turn form more ions by collision with the neutral atoms of the gas. Townsend introduced his second ionization coefficient γ by defining it as the cathode yield in electrons per incident ion. Since the electron multiplication must still follow Eq. (3.3), thus

$$n_a = (n_0 + n_+)\mathrm{e}^{\alpha d} \tag{3.7}$$

where n_0 is the number of the electrons per second from cathode due to external radiation; n_a number of electrons per second from all sources arriving at anode and n_+ number of the electrons per second from cathode by secondary emission. Considering that the difference between the number of electrons arriving at the anode and the number leaving the cathode shall equal the number of ions arriving at the cathode, we obtain

$$n_a - (n_0 + n_+) = \frac{n_+}{\gamma} \tag{3.8}$$

Combining Eq. (3.7) and Eq. (3.8), we have

$$n_a = n_0 \frac{\mathrm{e}^{\alpha d}}{1 - \gamma(\mathrm{e}^{\alpha d} - 1)} \tag{3.9}$$

or

$$i = i_0 \frac{\mathrm{e}^{\alpha d}}{1 - \gamma(\mathrm{e}^{\alpha d} - 1)} \tag{3.10}$$

The value of γ depends on the nature of the gas as well as on the electrode material, and varies widely, but it is always less than unity and values in the order of 10^{-2} are common.

When the number of electrons is sufficient to produce just enough ions to regenerate the number of lost electrons, a steady state is reached in which an equilibrium is established between the rate of formation of ions and the rate of their recombination with electrons. Eq. (3.10) shows that the Townsend current becomes theoretically infinite if

$$1 - \gamma(e^{\alpha d} - 1) = 0 \tag{3.11}$$

Since $\gamma \ll 1$, it can be given by

$$\gamma e^{\alpha d} = 1 \tag{3.12}$$

which is known as the Townsend criterion or the sparking criterion. At this stage, the discharge is self-sustaining. Extensive breakdown occurs in the gas and the glow discharge is thus established.

3.2 System configuration

The major structural components of plasma processing systems fall into the following basic configuration:

1. A vacuum chamber for the reaction;
2. A pumping system to provide the low pressure environment;
3. An energy source for plasma discharge;

4. A gas delivery system to introduce gas;

5. A control circuitry to regulate process parameters.

Figure. 3.1 shows a diagram of a home-built system we developed for plasma treatment in this study. It mainly consists of a plasma reactor, power supply, vacuum pumps, mass flow controller, pressure transducers, electric measurements and data acquisition system.

Reactor A reactor consists of a cylindrical stainless-steel chamber (Kurt J. Lesker, 10 inches in diameter and 12 inches in height) with a symmetrical plate-to-plate configuration of electrodes (stainless-steel plate with 9 cm in diameter). The maximum interelectrode distance is 10 cm. The upper electrode is grounded and the lower one is negatively polarized.

Power supply A Velonex 360 high power pulse generator is used for power supply. The frequency ν and the pulse width τ can be varied (1 Hz $\leq \nu \leq$ 300 kHz, 50 ns $\leq \tau \leq$ 3 ms) and the output pulse voltage is up to 2.5 kV. The DC pulsed power supply is externally triggered by an Agilent 33120A Functional Generator and delivers a DC voltage over a regulated glow discharge time and zero voltage over an afterglow discharge time.

Pumps The plasma reactors for materials processing normally operate at pressures between 10^{-4} and $\sim$ 10 Torr. However, lower background pressure is often required to ensure the cleanliness of the process. Therefore, the whole range of

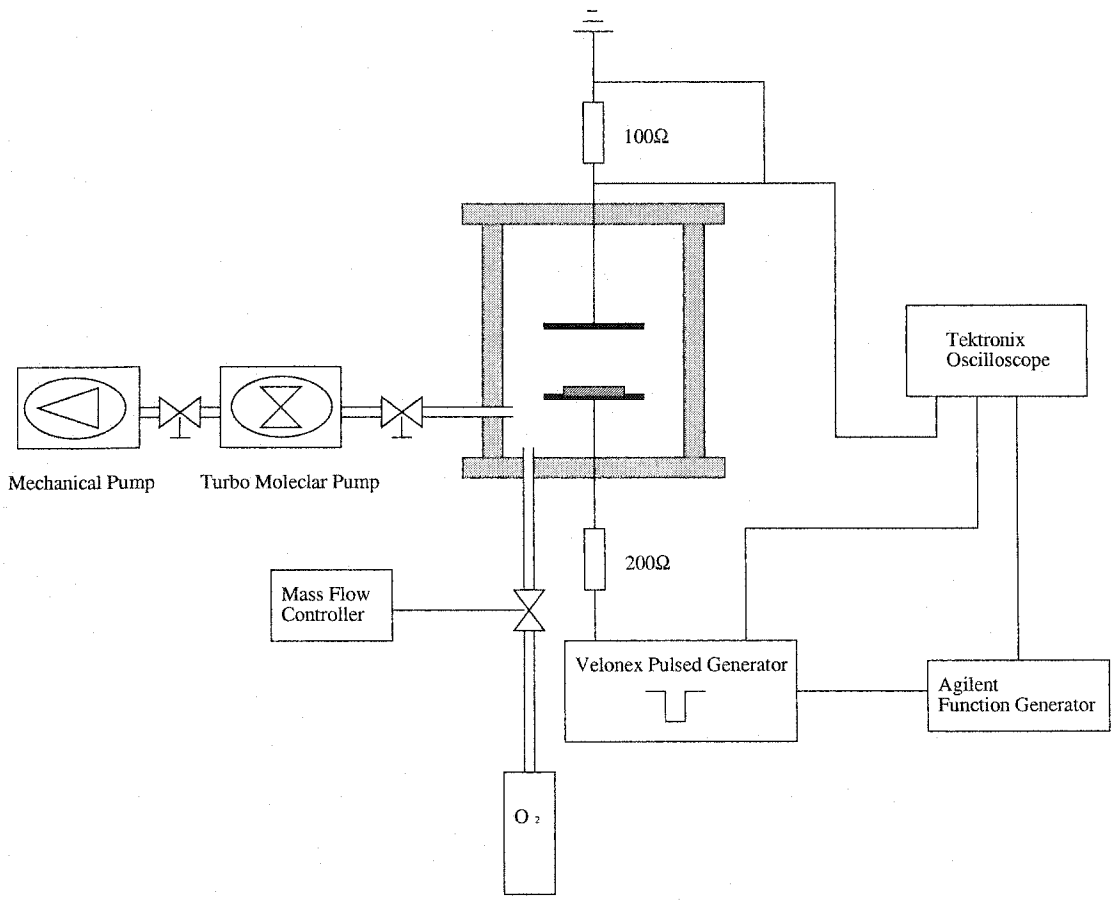

Figure 3.1: Schematic of an experimental set up for plasma treatment

vacuum is pumped by coupling of a Balzers turbomolecular pumps (TPH330) and a Leybold mechanical dry pump (EcoDry M15).

Mass flow controller The gases are supplied from standard Praxair gas cylinders and the flow rate is controlled by a mass flow controller (MKS, M100B) with a maximum flow rate of 500 sccm. The required flow rate is set by a HP 3497A Data Control Unit and can be read by a National Instruments 6024E Data

Acquisition Card.

Pressure regulation The chamber pressure is monitored by an ionization gauge at high vacuum (10^{-6} to 10^{-4} Torr) and by Capacitance Monometer MKS622 covering pressure from 2×10^{-3} to 10 Torr. The former one is read by Kurt J. Lesker IG4400 Ionization Gauge Controller and the latter is connected to a personal computer through the National Instruments Data Acquisition Card.

V-I measurements A digital oscilloscope (Tektronix TDS3014B) is used to visualize the $I - V$ signals of the discharge. The output of the power supply and the voltage across the electrodes are measured through two channels of the oscilloscope, while the latter is connected to a North Star voltage probe (PVM-2) as a potential divider. The current is detected through another channel by measuring the voltage drop across a resistance of 100 Ω connected in series with the electrodes.

Data acquisition system A HP 3497A Data Acquisition Unit installed with a HP44429A Digital-to-Analog Module is applied for setting the required gas flow rate. The actual mass flow rate and pressure values are collected by National Instruments 6024E Data Acquisition Card and then read by the personal computer. The process parameters can be controlled by the PC remotely through a visual Labview program.

The actual equipment apparatus of the developed system for plasma surface processing is presented in Fig. 3.2.

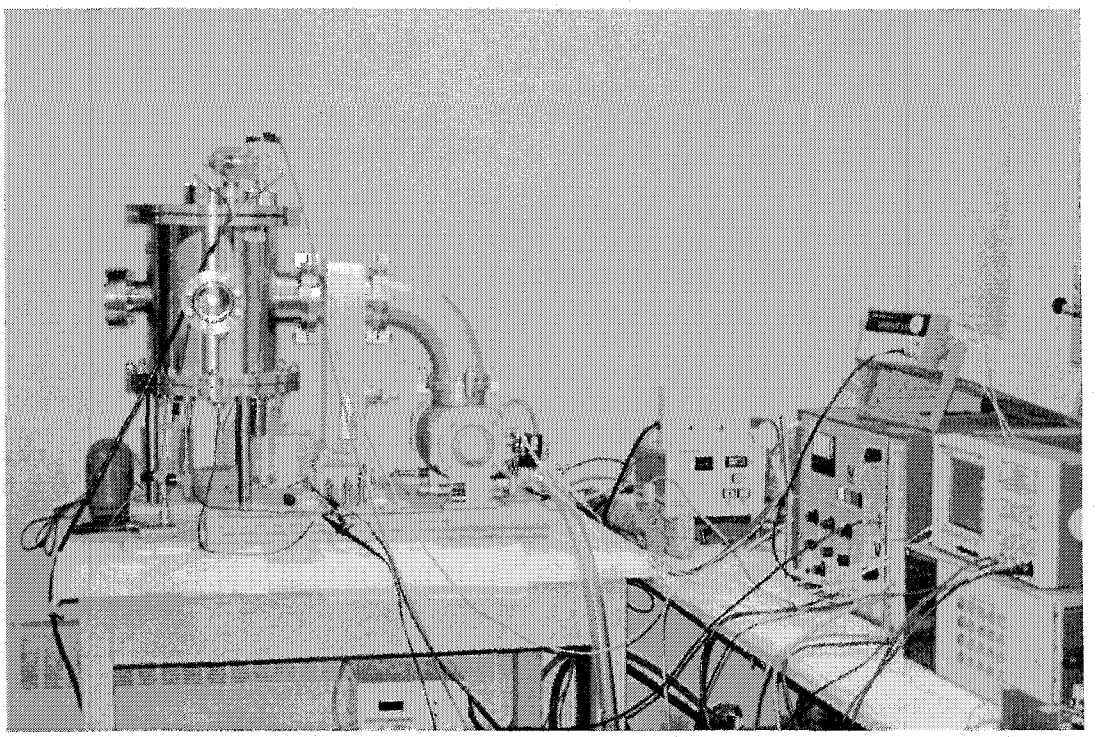

Figure 3.2: Actual equipment of the developed system for plasma surface processing

3.3 DC pulsed discharge

The cold plasma is usually excited and sustained electrically by direct current (DC), radio frequency (RF), or microwave (MW) power applied to a gas. Plasma chemistry in cold plasmas is controlled mainly by electron energies and gas temperatures. Therefore, as far as identical energies and temperatures can be achieved, the type of discharge used to create the plasma is of little importance. In this dissertation, a DC pulse plasma power source is applied during the experiments.

A DC pulsed discharge is very similar to a DC glow discharge, i.e. it can be

considered as a short DC glow discharge, followed by a generally longer afterglow, in which the discharge burns out before the next pulse starts [29]. Since a pulsed discharge can operate at much higher peak voltages and peak currents for the same average power as in a DC glow discharge, higher instantaneous sputtering, ionization and excitation can be expected, and hence better efficiencies. The typical duty cycle generally is very short, i.e. the ratio of 'pulse-on' period compared to 'pulse-off' period is very small. This means that the average electrical power is rather low, so that the sample will not excessively be heated.

Pulsed DC discharge also allows charged species to decay or recombination during the time off period of the pulse sequence. Plasma radicals, on the other hand, typically possess much longer lifetimes than ionic species generated in the plasma. Because of this lifetime difference, the substrate is primarily exposed to radical species in pulsed plasma systems. Thus, controlling the respective duration of the discharge time, during which active species are created, and the post-discharge time, where these species are still present, allows the inhibition of the switching from glow to arc regime as well as reducing sample sputtering.

Furthermore, varying the duration, duty cycle, input power and other characteristics of a pulsed discharge mode allows one to control rather easily the different plasma parameters. It is possible to control the substrate temperature with the pulse duty cycle without changing the plasma parameters during the pulse-on times. In fact, pusled excitation of the discharge presents the following advantages [30, 31, 32]:

1. It saves the energy needed for the process as the discharge voltage is zero during the afterglow;

2. It reduces arcing which is detrimental to the growing layer;

3. It limits the sample sputtering to only the discharge phase;

4. It provides more effective control by a variable duty cycle of active plasma regime and plasma afterglow.

In our experiments, the DC pulsed generator was used at a frequency ν of 1 kHz and a pulse duration time τ of 10 μs. The duty factor C_r is defined as the ratio between pulse duration time τ and pulsed voltage period T. Since $T = 1/\nu$, C_r was set at 1% by calculation as described in Fig. 3.3. This verifies that the pulse-on discharge period is relatively very short compared to the afterglow period.

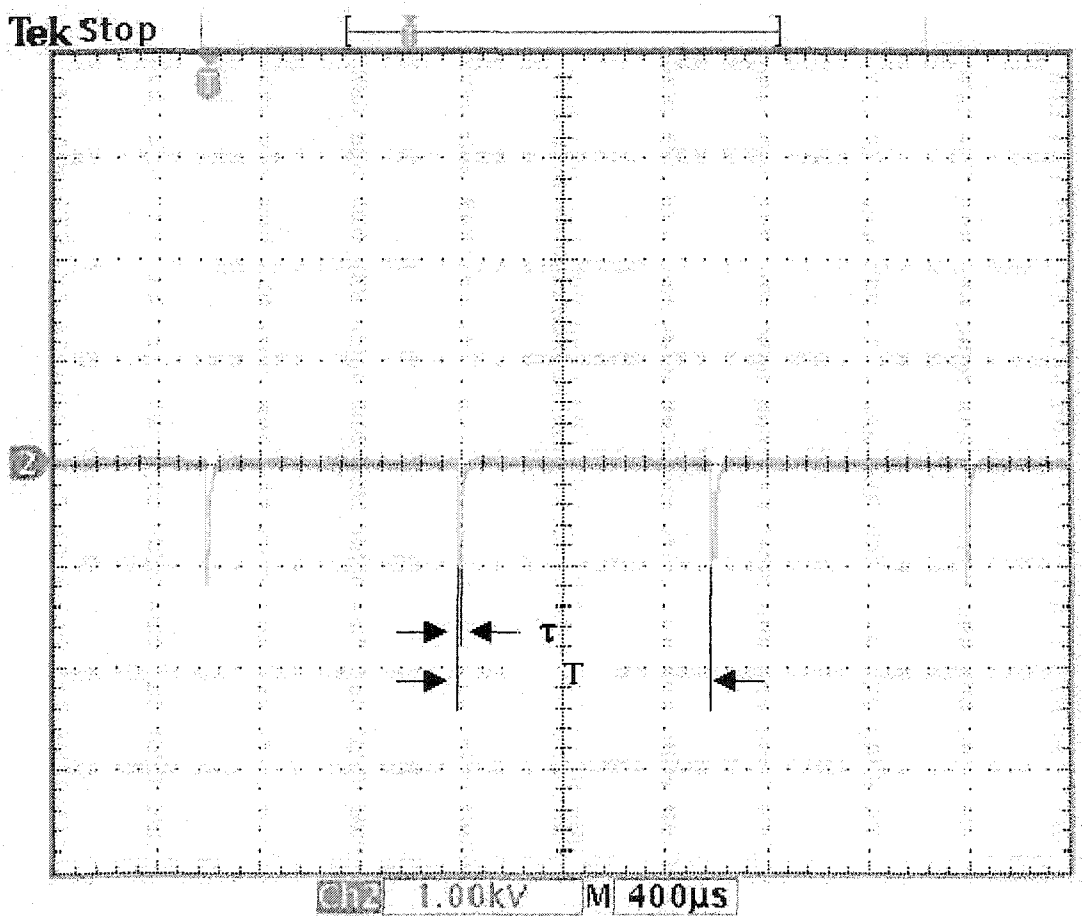

Figure 3.3: Definition of duty factor for a DC pulsed treatment

CHAPTER 4

SURFACE ANALYSIS TECHNIQUES

Plasma treatments typically modify extremely thin layers of the material surface within nanometer scale. In order to characterize the surfaces, a variety of surface sensitive techniques have been developed and improved over the last two decades. The main techniques utilized in this project to study the plasma modified surfaces will be described in this chapter.

4.1 Contact angle measurements

Contact angle measurement is a classical technique that provides information about surface tension or surface free energy of different materials. It is observed that, in most instances, a liquid placed on a solid surface will not wet it, but remains as a drop having a finite contact angle between the liquid and solid. Thus, contact angle measurement is easily performed by establishing the tangent (angle) of a liquid drop with a solid surface at the base. The attractiveness of using contact angles to estimate wettability and interfacial tensions is due to the relative ease with which contact angles can be measured on suitably prepared solid surfaces. It is apparent later that this seeming simplicity can be misleading [33].

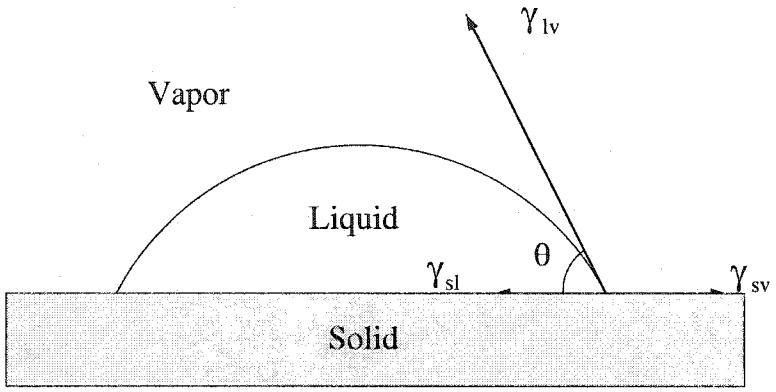

Figure 4.1: Schematic of three-interface contact angle system

The contact angle of a liquid drop on a solid surface is defined by the mechanical equilibrium of the drop under the action of three interfacial tensions (Fig. 4.1): solid-vapor, γ_{sv}, solid-liquid, γ_{sl}, and liquid-vapor, γ_{lv}. This equilibrium relation is known as Young's equation [34]:

$$\gamma_{lv} \cos\theta_Y = \gamma_{sv} - \gamma_{sl} \tag{4.1}$$

where θ_Y is the Young contact angle, i.e. a contact angle which can be inserted into Young's equation. Equation (4.1) implies a single, unique contact angle. However, contact angle phenomena are complicated in practice [35]. For example, the contact angle made by an advancing liquid (θ_a) and that made by a receding liquid (θ_r) are not identical. Nearly all solid surfaces exhibit contact angle hysteresis H defined by the difference between θ_a and θ_r:

$$H = \theta_a - \theta_r \tag{4.2}$$

Contact angle hysteresis can be caused by roughness and heterogeneity of a solid surface. In general, the experimentally observed apparent contact angle θ may or may not be equal to the Young contact angle θ_Y in that [36]:

1. On ideal solid surfaces, there is no contact angle hysteresis and the experimentally observed contact angle is equal to θ_Y;

2. On smooth, but chemically heterogeneous solid surfaces, θ is not necessary equal to the thermodynamic equilibrium angle. Nevertheless, the experimental advancing contact angle θ_a can be expected to be a good approximation of θ_Y;

3. On rough solid surfaces, no such equality between advancing contact angle and θ_Y exists. Thus, all contact angles on rough surfaces are meaningless in terms of Young's equation.

Considering DC pulsed plasma modified surfaces are smooth and chemically heterogeneous surfaces due to the inhibition of sputtering effect, we employed low-rate dynamic (advancing) contact angle measurements by an automated axisymmetric drop shape analysis−profile (ADSA-P) instead of goniometer measurements in the literatures.

ADSA-P is a technique to determine liquid-fluid interfacial tensions and contact angles from the shape of axisymmetric menisci; that is, from sessile as well as pendant drops [37]. Assuming that the experimental drop is Laplacian and axisymmetric, ADSA-P finds a theoretical profile that best matches the drop profile extracted from an image of a real drop, from which the surface tension, contact angle, drop volume, surface area, and three-phase contact radius can be computed. The strategy

employed is to fit the shape of an experimental drop to a theoretical drop profile according to the Laplace equation of capillarity, using surface/interfacial tension as an adjustable parameter. The best fit identifies the correct surface/interfacial tension from which the contact angle can be determined by a numerical integration of the Laplace equation. Details of the methodology and experimental setup can be found elsewhere [33, 38].

With respect to the low-rate dynamic contact angle measurements by ADSA-P, liquid was supplied to the sessile drop from below the wafer surfaces using a motorized syringe device. A schematic of this mechanism is shown in Fig. 4.2. A hole of about 1 mm diameter in the center of each wafer surface was made by using a diamond drill bit (Abrasive Technology, cat# 261.8C) in order to facilitate such a procedure. To avoid leakage between a stainless steel needle and the hole, Teflon tape was wrapped around the end of the needle before inserting into the hole.

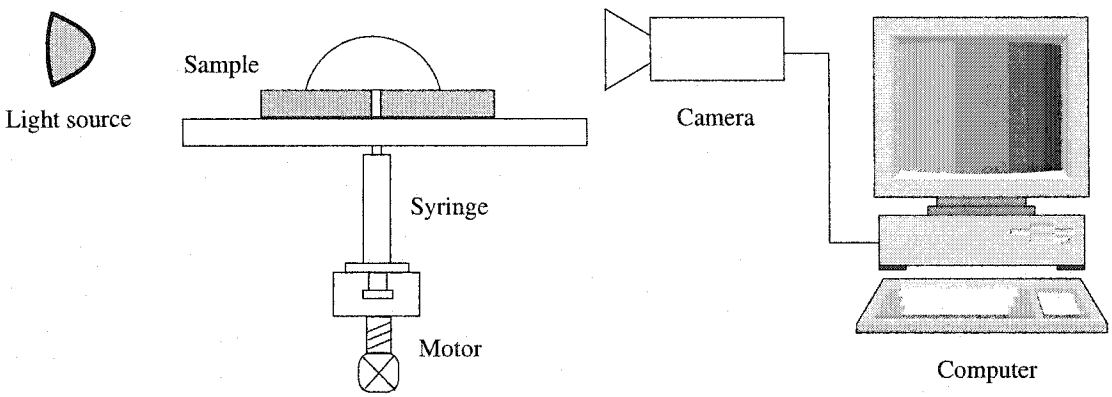

Figure 4.2: Schematic of ADSA-P dynamic contact angle measurements.

In actual experiments, an initial liquid drop of about 0.3 cm radius was carefully

deposited, covering the hole on the surface. This is to ensure that the drop will increase axisymmetrically in the center of the image field when liquid is supplied from the bottom of the surface and will not hinge on the lip of the hole. Then, deionized water was pumped by a motorized-syringe from below at a velocity of the three-phase contact line less than 1 mm/min. A sequence of pictures of the growing drop was then recorded by the computer typically at a rate of 1 picture every 1 s, until the three-phase contact radius was about 0.5 cm or larger. For each low-rate dynamic contact angle experiment, at least 50 and up to 200 pictures were normally taken. Since ADSA-P determines the contact angle and the three-phase contact radius simultaneously for each picture, the advancing dynamic contact angles as a function of the three-phase contact radius (i.e., location on the surface) can be obtained.

This method has an additional advantage: the quality of the surface is observed indirectly in the measured contact angles. If a solid surface is not very smooth, irregular and inconsistent contact angle values will be seen as a function of the three-phase contact radius. When the measured contact angles are essentially constant as a function of surface location, the mean contact angle for a specific rate of advancing can be obtained by averaging the contact angles, after the three-phase contact radius reaches 0.4 to 0.5 cm.

4.2 Zeta potential determination

The zeta potential, formally defined as the electrical potential at a electrokinetic plane of shear, is an important property of charged solid-liquid interfaces due to its ability to characterize the charge states and electrokinetic properties of surfaces.

When in contact with a liquid medium, most solid surfaces may be charged and surrounded by the ions of opposite sign from the liquid phase. The rearrangement of the charges on the solid surface together with the balance of charges in the liquid give rise to what is known as the electric double layer, EDL. In simple term, its name came about because of the separation of charge between the surface and the electrolyte solution. One layer is the charge on the surface, and the other, a "layer" of ions in the vicinity of the surface [39].

The concept of electric double layer was proposed by Helmholtz [40] over a century a ago. Gouy [41] and Chapmen [42] independently introduced the theory of diffusion layer. At present, Gouy-Chapman-Stern-Graham model (GCSG) is widely accepted [43]. According to the GCSG model, the electrical double layer is divided into the inner (IHP), outer (OHP) Helmholtz planes and the diffuse layer. When an external force field is applied to the solid/liquid system, a relative movement of the liquid and solid phase occurs. This leads to a charge separation in the electrical double layer. Ions underlying a higher attractive force than the external force remain on the solid surface while charge carriers which are bounded more weakly move with the liquid phase. Normally, the zeta potential is referred to the electrical potential of the shear plane, where charge separation takes place. Therefore, the zeta potential reflects the force balance between the external force and the interaction forces between ions and the solid surface. In other words, zeta potential represents the strength and polarity of the electric double layer.

Zeta potentials formed on flat plates are commonly determined by streaming potential and streaming current methods. Figure. 4.3 presents a home-built device

based on a streaming potential/current technique employed in this study. The device system consists of a parallel-plate microchannel, a liquid flow loop (including a pump and flow rate meter), pressure transducer and an electrometer (Keithley, 6517A). Microscope glass slides (Fisher, cat# 12-550A) were selected for PMMA coating and plasma modification as components for assembly into a rectangular microchannel. Two parallel glass plates were separated by thin plastic shims (Small Parts Inc., FL) as spacers for the channel walls. Details of the measurement setup can be found elsewhere [44].

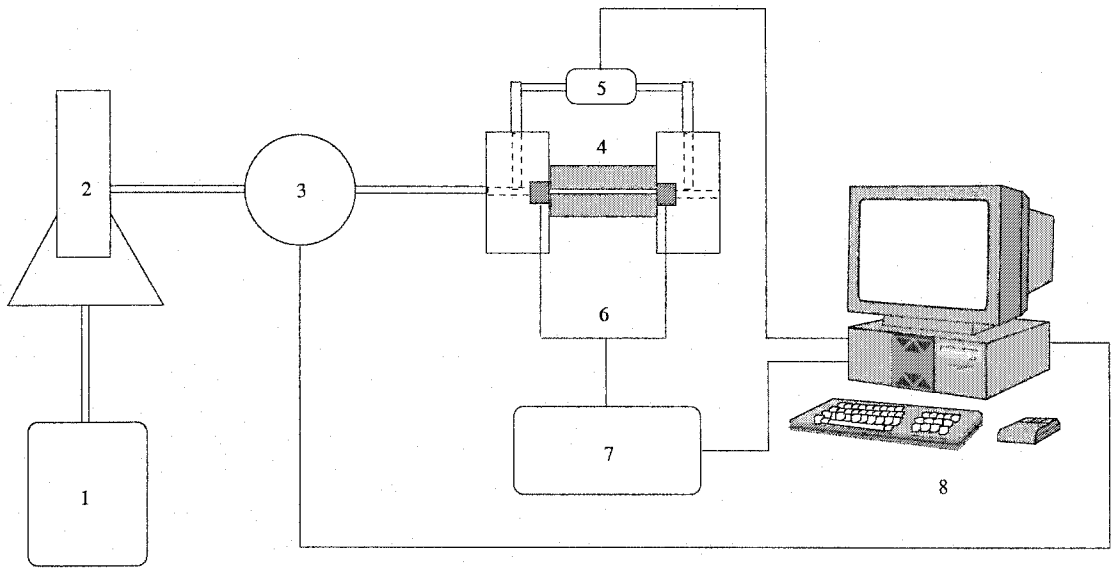

Figure 4.3: Schematic of zeta potential measurements of the parallel-plate microchannel: 1. Liquid reservoir; 2. Syringe pump; 3. Flowmeter; 4. Parallel-plate microchannel; 5. Pressure transducer; 6. Ag electrodes; 7. Electrometer; 8. Data acquisition system.

When a liquid is forced to flow through a microchannel under an applied hydro-

static pressure, the counterions in the diffuse layer (mobile part) of the EDL are carried toward the downstream, resulting in an electrical current I_s in the pressure-driven-flow direction, which is termed the streaming current. The accumulation of excess charges down-stream causes the build-up of an electric field which drives an electric current back (by ionic conduction through the liquid) against the direction of the liquid flow. A steady state is quickly established, and the measured potential difference across the microchannel is called the streaming potential U_s [45]. The zeta potential ζ can be obtained from either U_s or I_s according to, respectively,

$$\zeta(U_s) = \frac{\eta(K_B + 2K^\sigma/h)}{\varepsilon_0 \varepsilon_r} \frac{dU_s}{dp} \tag{4.3}$$

or

$$\zeta(I_s) = \frac{\eta L}{\varepsilon_0 \varepsilon_r bh} \frac{dI_s}{dp} \tag{4.4}$$

where η is the dynamic viscosity of the fluid, K_B is the specific bulk conductivity of the fluid and K^σ is the surface conductivity; while ε_0 is the permittivity of vacuum and ε_r is the relative dielectric permittivity of the streaming solution. Finally, L, b and h are the length, width and height of the channel, respectively. The width and length of the microchannel were measured by using a precision gauge (Mitutoyo, Japan, Model CD-6B) with an accuracy of 1 μm. For laminar flow without electrokinetic effect, the dependence of the volume flux Q in a slit channel on its geometry is given by

$$Q = \frac{pbh^3}{12\eta L} \tag{4.5}$$

Hence the slit channel height h can be calculated from the measured fluid flow Q and

known pressure differences p with an external short circuit to remove electrokinetic effect:

$$h = \sqrt[3]{\frac{12\eta LQ}{pb}} \tag{4.6}$$

The streaming potential and streaming current values for a given channel height h can be used to calculate the surface conductivity K^{σ} [46]:

$$K^{\sigma} = \frac{L}{2b}\frac{I_s}{U_s} - \frac{K_B}{2}h \tag{4.7}$$

4.3 X-ray Photoelectron Spectroscopy (XPS)

X-ray Photoelectron Spectroscopy (XPS), also called electron spectroscopy for chemical analysis (ESCA), is a powerful tool for studying plasma-induced chemistry at the modified surface because of its surface sensitivity (1-10 nm), combined with quantitative and chemical state identification capability [47].

The phenomenon is based on the photoelectron effect explored by Einstein in 1905 where electrons can be ejected from a surface when photons impinge upon it. Photoelectrons are emitted from the surface of the material as a result of absorption of a photon with energy $E = h\nu$. The inner core-level electrons can be photoionized using X-ray photons and these photoelectrons are ejected with discrete kinetic energy E_K given by

$$E_K = h\nu - E_B - \phi \tag{4.8}$$

where E_B is the binding energy of the photoelectron relative to the Fermi level, and

ϕ is the work function of the spectrometer. The Fermi level is used as the zero binding energy level by definition. Since the kinetic energy of the photoelectron is a "fingerprint" of the elements present and their chemical environment, XPS provides elemental specificity and a measurement of the chemical environment of the elements.

In XPS, Al $K\alpha$ (1486.6 eV) and Mg $K\alpha$ (1253.6 eV) are often used as soft x-ray sources to irradiate a sample material in high vacuum (typically $\leq 10^{-9}$ Torr), producing photoionization and ejected free electrons. The energy of the photoelectrons leaving the sample is determined using a multi-channel analyzer and this gives a spectrum with a series of photoelectron peaks. The shape of each peak and the binding energy can be slightly altered by the chemical state of the emitting atom; thus the peak areas can be used to determine the composition of the material surface. XPS is not sensitive to hydrogen or helium, but can detect all other elements.

In this study, XPS spectra and the atomic concentrations of the sample surfaces were acquired on a Kratos Axis 165 photoelectron spectrometers using a monochromatic aluminum X-ray source (Al $K\alpha$ 1486.6 eV) operating at 210 W (15 kV, 14 mA). The analyzed surface area was 1 mm in diameter and the photoelectron take-off angle (with respect to the surface normal) was held at 90°. The instrument was calibrated to the $4f_{7/2}$ peak of gold at $E_B = 84.0$ eV. The base pressure was 2×10^{-10} Torr with an operating pressure of 2×10^{-9} Torr. Charge compensation was accomplished using low energy electrons. Standard operating conditions for good charge compensation are -2.8 V for the bias voltage, -1.0 V for the filament voltage, and 2.1 A for the filament current. The hemispherical analyzer functioned at a constant pass energy of 20 eV for high resolution spectra and 150 eV for quantitative analysis.

Preliminary data analysis and quantification were performed using a VISION software provided by the manufacturer. The C 1s and O 1s envelopes were fitted using asymmetrical 70% Gaussian and 30% Lorentzian component profiles after subtraction of baseline using a linear background. Binding energies (BE) were determined by reference to the C 1s BE (284.6 eV) prior to peak fitting.

The samples were cut to a size of $\sim 1 \times 1$ cm^2 and clamped to the sample holder with metal clamps directly before introduction into the instrument. It is worth mentioning that the samples were plasma-treated in our laboratory and then transferred to another laboratory in a different department for analysis. Thus, minute exposure of the treated substrates to atmosphere is inevitable.

4.4 Scanning electron microscopy (SEM)

Scanning electron microscopy (SEM) is an imaging technique to characterize specimens with regard to their topographical features. SEM creates the magnified images by using electrons instead of light waves. A beam of electrons is produced at the top of the microscope by an electron gun. The beam travels through electromagnetic fields and lenses, which focus the beam down toward the sample. The incident electrons cause low energy secondary electrons to be generated, while some escape from the surface. A detector counts these emitted electrons and sends the signals to an amplifier. The final image is built up from the number of electrons emitted from each spot on the sample. The combination of higher magnification, larger depth of focus, higher resolution, and ease of sample observation makes the SEM one of the most heavily used instruments in research areas today [48].

However, SEM has been adopted rarely to observe organic monolayers owing to the very small topographic difference (less than several nanometers) for a long time [49]. Recent evaluations show that it is also suitable for the study of thin organic layers on flat solid supports; i.e., specimens that possess almost no topographic details. Contrast phenomena, other than the well-known topographic features, allow for the characterization of thin organic layers. For example, properties contributing to these contrasts are differences in chemistry, local film thickness, orientation or molecular packing of the monolayers [50].

SEM is capable of generating images of two-dimensional patterns of self-assembled monolayers (SAMs) of alkanethiolates adsorbed onto gold [51]. In Chapter 6, images of plasma patterned SAMs were acquired in the secondary electron detection made of a LEO 1430 scanning microscope, using an accelerating voltage of 3.5 kV, an emission current of 2 μA and a collection voltage of 300 V. The electron beam was slowly scanned for an exposure time of 1.3 min over the samle area which were prepared without performing conductive overcoating.

4.5 Optical profilometer

White light interferometry is a powerful technique for non-contact measurement of surface topography at a high vertical and moderate lateral resolution. In this study, surface morphology of the plasma treated substrate was observed by means of an optical profilometer (Zygo, New View 5000). Based on this technique, a pattern of bright and dark lines (fringes) results from an optical path difference between a reference and a sample beam.

Table 4.1: Characterization techniques used for plasma treated surface

Analytic tools	Surface properties
advancing contact angle	wettability and surface tension
streaming potential/current	charge state and zeta potential
XPS	chemical composition
SEM	topography and composition
optical profilometer	topography and roughness

This three-dimensional surface structure analyzer employs scanning white light for imaging and allows measurements of microstructure and topography of surfaces. Such a device consists of a microscope, an interferometric objective and a high-resolution camera. An incoming light is split inside an interferometer with one beam going to an internal reference surface and the other to the sample. After reflection, the beams recombine inside the interferometer, undergoing constructive and destructive interference and producing light and dark fringe patterns; a precision vertical scanning transducer together with a camera generate a three-dimensional interferogram of the surface, which is processed by the computer and transformed by frequency domain analysis to result in a quantitative 3-D image.

In conclusion, a combination of surface analysis techniques were employed to obtain composition and structural information of plasma modified surfaces. Each measurement probes a unique property of the material surface by different physical processes (Table 4.1). Therefore, a complete picture can then be constructed.

Chapter 5

Plasma-based surface modification on PMMA

In this section, PMMA substrates were treated under a DC pulsed oxygen plasma for different treatment times. The modified surface properties were investigated by multiple surface analytic techniques including contact angle, zeta potential, XPS and optical profilometer measurements. The effect of chemical structure and surface charge on the wettability modification and their relationships will be discussed.

5.1 Material preparation

The PMMA films were made by spin-coating methods. Polymethyl methacrylate (PMMA) was purchased from Polysciences (Warrington, P.A., cat# 04553, M_W = 75,000) as 200 μm beads. A 2% PMMA/chloroform solution was prepared using chloroform (Fisher chemicals: C297-4, 99.9%) as the solvent. Silicon wafers $< 100 >$ (Wafer World, West Palm Beach, FL; test grade) were selected as the substrate for the polymer coating. They were obtained as circular discs of 10 cm diameter and were cut into rectangular wafer surfaces of about 2.5 cm $\times$ 4.5 cm. Each slide was soaked in chromic acid for at least 24h, rinsed with doubly distilled water, and dried under a heat lamp before the polymer coating. The PMMA/chloroform solution was

casted onto the wafer mounted on the chunk of the spinner; the spinner was set to rotate at the spinning rate 2000 rpm for 50 seconds. A thin layer of PMMA that is less than 1 μm was formed on the slide surface after evaporation of the chloroform.

5.2 Experimental parameters

Basically, the properties of materials processed by plasma depend on the internal parameters of plasma. However, only the external parameters or process conditions are adjustable and controllable. A wide variety of processing parameters can directly affect the chemical and physical characteristics of a plasma and subsequently affect the surface properties obtained by plasma modification. Figure. 5.1 shows schematically the basic relationships among the internal parameters, external parameters and the resultant properties of processed materials.

For a given plasma system, power, pressure and flow rate are the widely used process variables and their influence on plasma is significant. In general, increasing the power increases the plasma density and eventually increases the particle interaction rates. The gas pressure in the system determines the free path of species in the plasma. A short mean free path has two main effects: lower electron energy, and more gas phase reactions as a result of increased collisions in the plasma. A parameter which depends directly on flow rate is the residence time τ of a gas molecule, i.e. the mean time that remains in the process chamber before being pumped away. It can be given by [15]

$$\tau = \frac{PV}{Q} \tag{5.1}$$

where P is the pressure, V is the volume of the reactor, and Q is the pumping speed

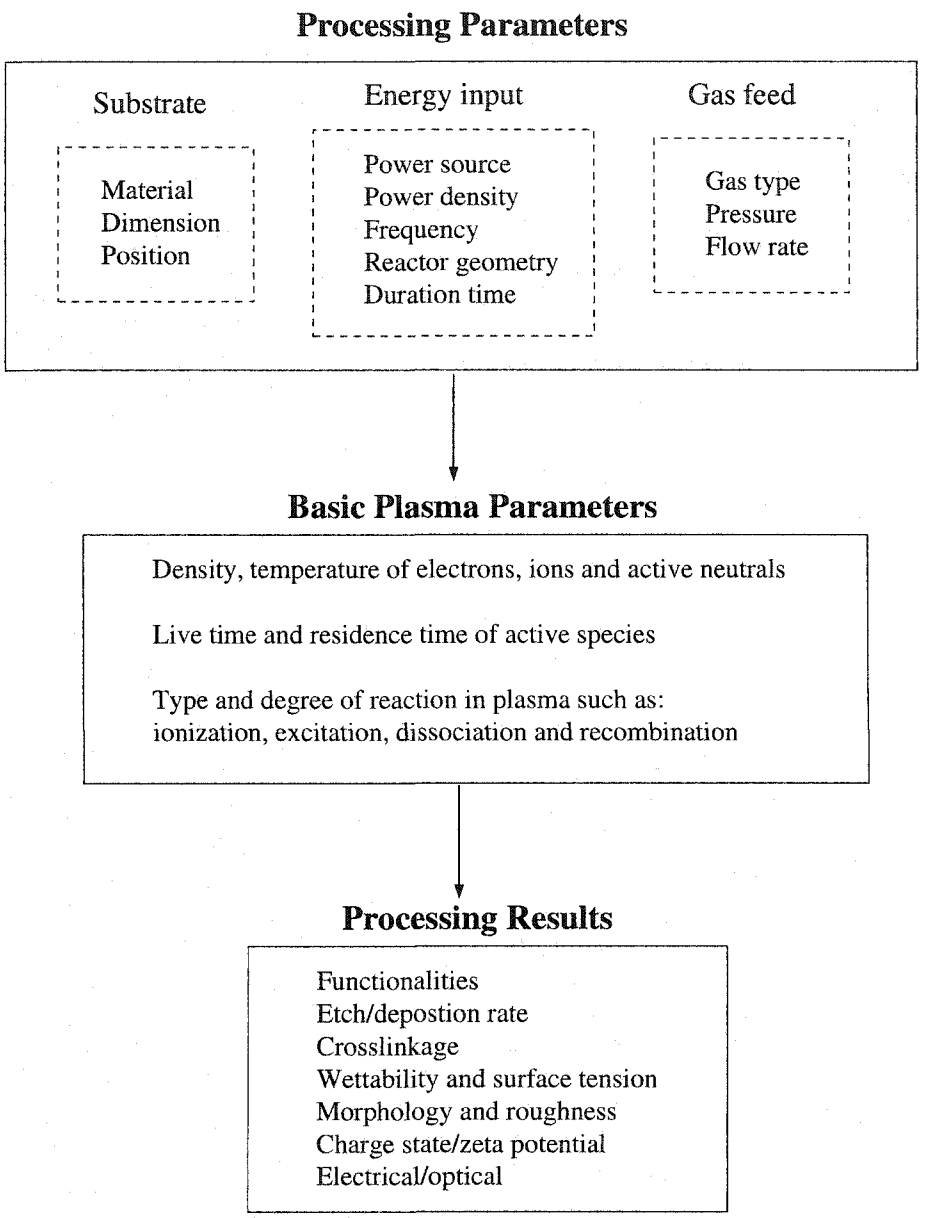

Figure 5.1: Relations among internal, external parameters and the resultant surface properties

in unit of Torr-liters/sec. Thus, the residence time is roughly in inverse proportion with the flow rate if the pressure remains constant. However, the influence of flow rate on plasma composition also depends on the location and configuration of the inlet.

In this experiment, the interelectrode distance was fixed at 4 cm. The power supply delivers DC pulses with the pulse width of 10 μs and a frequency of 1 kHz. The negative pulse voltage magnitude was 1000 V during the treatment. The PMMA slides were installed on the lower plane electrode and treated with an oxygen plasma. The reactor was evacuated to a base pressure of 2×10^{-5} Torr and then O_2 gas was introduced into the chamber. The operating pressure is maintained at 0.2 Torr with gas flow rate at 10 sccm during the treatment. The PMMA slides were treated from 1 s to 50 s for enhanced wettability.

5.3 Results

5.3.1 Contact angle and surface tension

The process is known as wetting when a liquid such as water increases its area of contact with a solid substrate. A quantitative means of evaluating the surface wetting tendency is the measurement of contact angle.

Figure. 5.2 displays a typical experimental result of ADSA-P water contact angle of untreated PMMA. As can be seen in this figure, there was an initial increase in the contact angle at essentially constant three-phase contact radius as the drop volume increased. This results from the fact that even carefully putting an initial liquid drop from above on a solid surface can result in a contact angle somewhere between

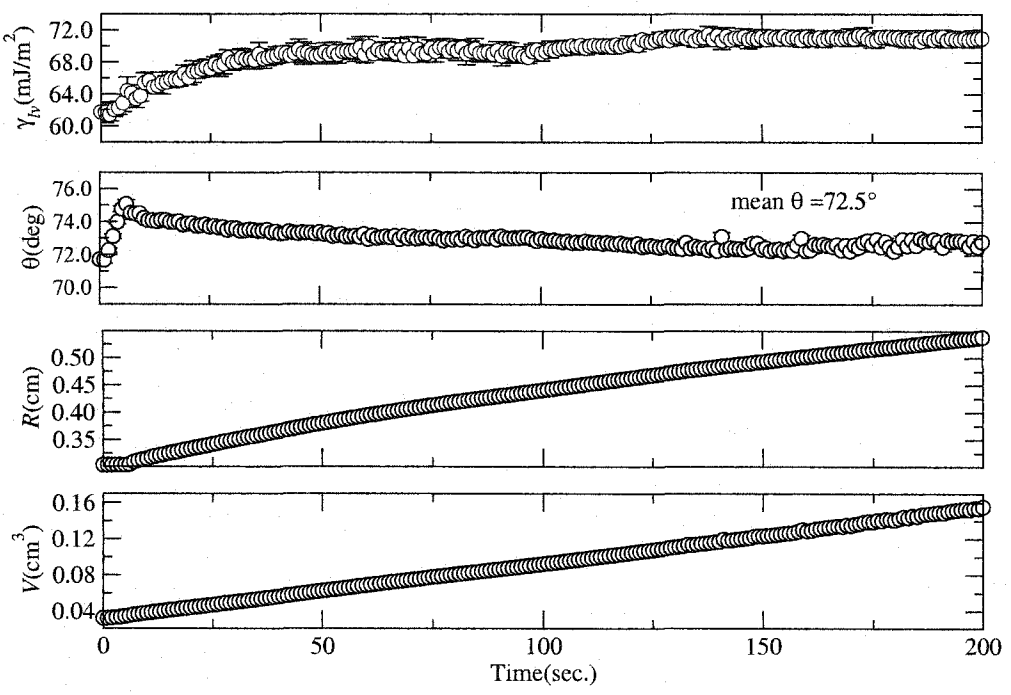

Figure 5.2: Low rate advancing contact angles on PMMA for water.

advancing and receding. The contact angles are essentially constant, as the drop volume V further increases and hence the three-phase contact radius R. Increasing the drop volume in this manner ensures the measured θ to be an advancing contact angle. It should be noted that the measured contact angles were essentially constant as R increases. This indicates good surface quality of the surfaces used. The averaged contact angle of 72.5° is consistent with the literature values [36, 52].

The advancing contact angles for water against different treatment times for plasma modified PMMA surfaces are shown in Fig. 5.3. The applied voltage was maintained at 1 kV during the discharge treatment. Measurements were made immediately after the treatment. The contact angle decreases rapidly with treatment time and remains essentially constant after about 5 s of treatment. The calculation of solid surface tension γ_{sv} from the contact angle of a liquid of surface tension γ_{lv} starts with Young's equation (4.1) and an equation of state [33]

$$\gamma_{sl} = \gamma_{lv} + \gamma_{sv} - 2\sqrt{\gamma_{lv}\gamma_{sv}}(1 - \beta(\gamma_{lv} - \gamma_{sv})^2) \tag{5.2}$$

where β takes the value of 0.0001057 $(\mathrm{m}^2/\mathrm{mJ})^2$. Note that a γ_{lv} value of 72.70 $\mathrm{mJ/m}^2$ for water is used. Combining Eqs. (4.1) and (5.2) yields

$$\gamma_{lv}(1 + \cos\theta_Y) = 2\sqrt{\gamma_{lv}\gamma_{sv}}(1 - \beta(\gamma_{lv} - \gamma_{sv})^2) \tag{5.3}$$

where the value of γ_{sv} can be determined from a pair of experimentally determined γ_{lv} and θ; the corresponding γ_{sl} value can then be calculated from either Eq. (4.1) or (5.2). Table 5.1 shows the computed γ_{sv} and γ_{sl} values for untreated PMMA and oxygen-plasma treated PMMA corresponding to the advancing contact angles of water. The untreated PMMA surface exhibits a contact angle of 72.5°, which is associated with a solid-vapor surface tension value of 40.1 $\mathrm{mJ/m}^2$. After a discharge treatment of 1 s, the contact angle of PMMA decreases rapidly to 61.5° as a result of surface modification through oxygen plasma. For a treatment time of 2 s, the contact angle decreases from 61.5° to 56.4°. From the surface tension, there is an apparent increase of γ_{sv} from 46.9 $\mathrm{mJ/m}^2$ for 1 s treatment time to 52.8 $\mathrm{mJ/m}^2$ for 5 s, which

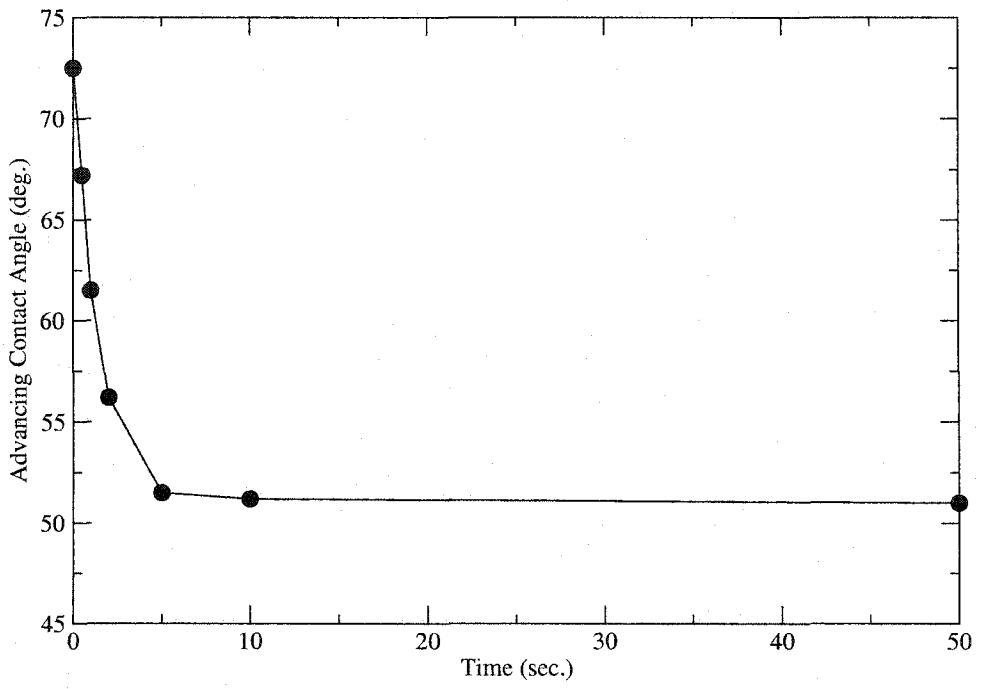

Figure 5.3: Wettability of O_2 plasma modified PMMA.

indicates the influence of treatment time on the contact angle and, as a consequence, on the surface tension. Table 5.1 also shows the remaining contact angles for other treatment times longer than 5 s; no significant change in the contact angle, and hence the surface tension is apparent.

Table 5.1: Experimental contact angles and calculated surface tensions of O_2 plasma treated PMMA without consideration of EDL effect

Treatment (s)	Contact angle (deg.)	γ_{sv} (mJ/m^2)	γ_{sl} (mJ/m^2)
0	72.5	40.1	18.2
1	61.5	46.9	12.2
2	54.2	51.2	8.7
5	51.5	52.8	7.6
10	51.2	53.0	7.4
50	51.0	53.1	7.4

5.3.2 Zeta potential measurements and evaluation

For a given streaming liquid, after the completion of the streaming potential and streaming current measurements of each channel for a specific liquid and flow rate, the averaged values from a total of 10 readings for p and I_s were used in Eq. (4.4) to determine the zeta potential ζ. Figure. 5.4 shows the dependence of zeta potential on the films versus the treatment time of oxygen plasma discharge. It can be seen that a strong increase in ζ takes place within the first 5 s; after that, the curve flattens out, reaching a value of about -86 mV. The shape of curve is also similar to that of contact angle in Fig. 5.3.

It is well known that zeta potential depends on the surface charge density and double layer thickness of different electrolyte solutions. The surface charge density σ can be related to the zeta potential by solving the nonlinear Poisson-Boltzmann equation for an electrolyte with a symmetrical $z_0 : z_0$ valence [53]:

$$\nabla^2\psi = \frac{2n_\infty z_0 e}{\varepsilon_0\varepsilon_r}\sinh\frac{z_0 e\psi}{kT} \tag{5.4}$$

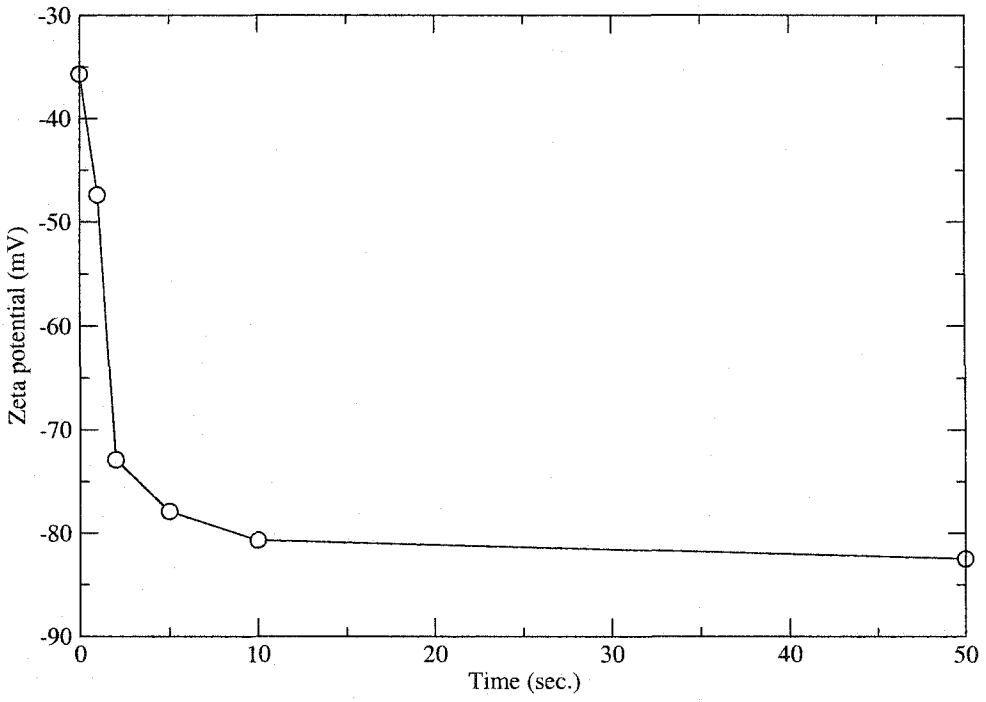

Figure 5.4: Zeta potential versus treatment time for O_2 plasma modified PMMA.

where z_0 is the valence of the symmetrical electrolyte, e is the elementary charge, n_∞ is the ionic concentration in an equilibrium electrochemical solution at the neutral state with $\psi = 0$, k is the Boltzmann constant and T is the absolute temperature. For one dimension consideration, this can be integrated by multiplying both sides by

$2(d\psi/dx)$:

$$\frac{2d\psi}{dx}\frac{d^2\psi}{dx^2} = \frac{4n_\infty z_0 e}{\varepsilon_0\varepsilon_r}\sinh\frac{z_0 e\psi}{kT}\frac{d\psi}{dx} \tag{5.5}$$

Integrating from $\psi = 0$ to some point in the double layer yields

$$(\frac{d\psi}{dx})^2 = \frac{4n_\infty kT}{\varepsilon_0\varepsilon_r}[\cosh\frac{z_0 e\psi}{kT} - 1] \tag{5.6}$$

Using the identity $\cosh p = 2\sinh^2(p/2) + 1$, Eq. (5.6) becomes

$$\frac{d\psi}{dx} = -\frac{2\kappa kT}{z_0 e}\sinh\frac{z_0 e\psi}{2kT} \tag{5.7}$$

where κ is defined as the reciprocal of the double layer thickness for a $(z_0 : z_0)$ electrolyte:

$$\kappa = (\frac{2n_\infty z_0^2 e^2}{\varepsilon_0\varepsilon_r kT})^{1/2} \tag{5.8}$$

On the other hand, the total charge density σ per unit area of surface at the plane $x = d$ in the diffuse layer is given by

$$\sigma_d = \int_d^\infty \rho dx \tag{5.9}$$

where ρ is the volume density of charge. By means of the Poisson equation,

$$\nabla^2\psi = -\frac{\rho}{\varepsilon_0\varepsilon_r} \tag{5.10}$$

Eq. (5.9) becomes

$$\sigma_d = \int_\infty^d \varepsilon_0\varepsilon_r\frac{d^2\psi}{dx^2}dx = \varepsilon_0\varepsilon_r[\frac{d\psi}{dx}]_\infty^d \tag{5.11}$$

Table 5.2: Experimental values of ζ and σ for untreated and 50 s treated PMMA in different electrolyte solutions

Sample	solution	ζ (I_s) (mV)	σ (μC/cm^2)
Untreated	water	-35.9	-0.0089
	0.1 mM KCl	-13.4	-0.031
	1 mM KCl	-7.5	-0.055
50 s Treated	water	-82.5	-0.028
	0.1 mM KCl	-48.5	-0.130
	1 mM KCl	-20.9	-0.157

As $(d\psi/dx)_{x\to\infty} = 0$, Eq. (5.11) reduces to

$$\sigma_d = -\frac{2\varepsilon_0\varepsilon_r kT\kappa}{e}\sinh\frac{z_0 e\psi_d}{2kT} \tag{5.12}$$

Knowing that the surface potential at the shear plane is ζ, we obtain the corresponding surface charge as

$$\sigma = -\frac{2\varepsilon_0\varepsilon_r kT\kappa}{e}\sinh\frac{z_0 e\zeta}{2kT} \tag{5.13}$$

The zeta potential and corresponding interfacial charge density of untreated and 50 s plasma-treated PMMA in different solutions are given in Table 5.2. The plasma treatment obviously causes an increase in the value of zeta potential and interfacial charge density for all solutions due to a strong EDL.

5.3.3 Surface Chemistry

The XPS spectrum shows the chemical composition in the top layer of the materials. Figure. 5.5 presents the survey spectra (0 to 1000 eV) of the original PMMA surface. The two peaks represent carbon and oxygen elements, respectively, showing that no

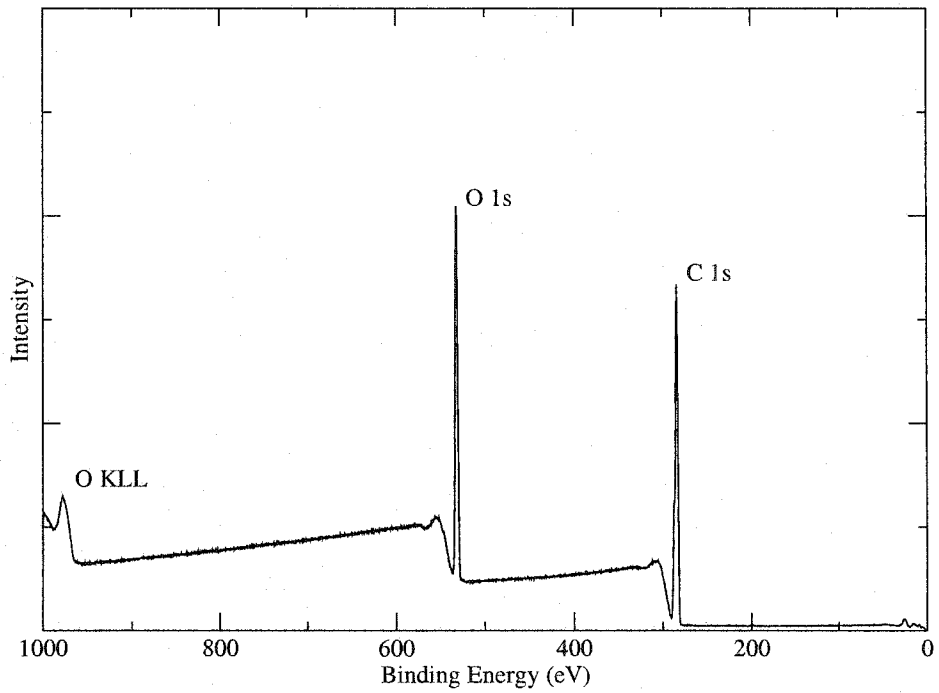

Figure 5.5: XPS survey spectra of PMMA.

other contamination is involved.

The high resolution spectra of C1s peak can show the fine structure of carbon atoms. By using deconvolution method with distinctive binding energies, one can obtain the relative concentrations of the carbon bonding structures related to the surface functional groups. The fitted high resolution C1s core-level photoemission spectra of untreated PMMA together with a representation of the chemical structure

Table 5.3: Fitting parameters of the C1s envelope of PMMA

Peak No.	BE (eV)	FWHM (eV)	Area (%)
1	284.6	0.95	36.4
2	285.2	0.95	23.0
3	286.3	1.10	22.0
4	288.6	0.85	18.6

of the monomers are presented in Figs. 5.6 and 5.7, respectively.

The peak labels in the spectra correspond to the carbon atoms having different environments in the monomers which can be decomposed into four distinct components [54]: C1s (1) calibrated at a binding energy of 284.6 eV corresponds to carbon atoms involved in the C–C and C–H bonds of the PMMA; C1s (2) at 285.2 eV corresponds to the quaternary carbon atom in α-position to the ester group; C1s (3) at 286.3 eV is the carbon atom involved in the methoxy group of the ester chemical function and C1s (4) at 288.6 eV is the carbon atom of the carboxylic group (O–C=O). The fits were based on reference measurements of Kratos [55], and were performed by keeping the binding energies and widths of the peaks identical to the literature values, while varying the intensities. The binding energies and the relative area of the fitted peaks are given in Table 5.3.

When the PMMA samples were treated with a O_2 plasma, the structure of the C1s spectra was greatly affected. The differences in the shape of the C1s spectra reveal strong modifications of the elemental composition for the PMMA surface (cf Fig. 5.8). Decomposition of the C1s peak reveals the increased area corresponding to polar functional groups and the presence of two new components: C1s (5), located at

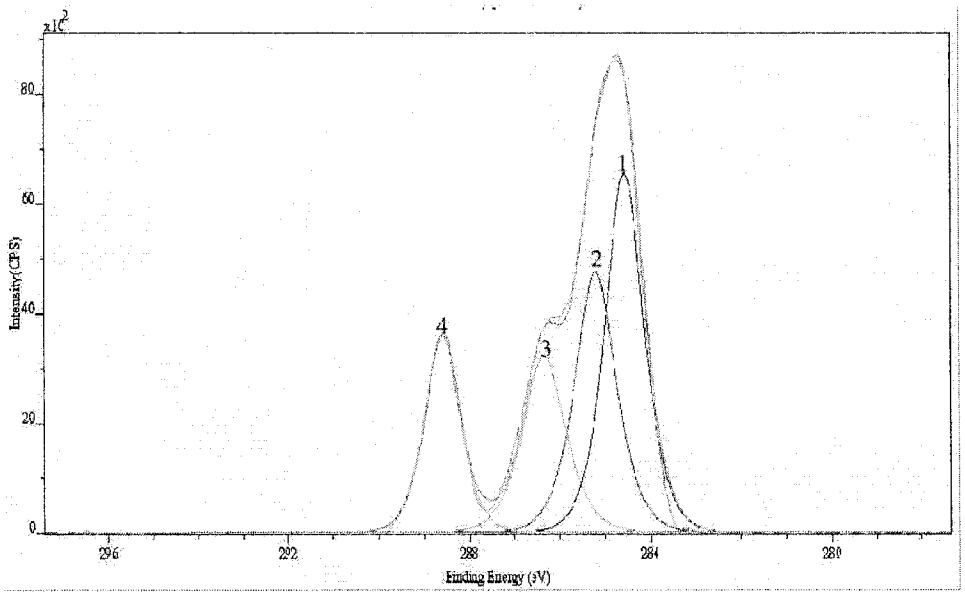

Figure 5.6: C1s XPS spectra of PMMA with fitted peaks.

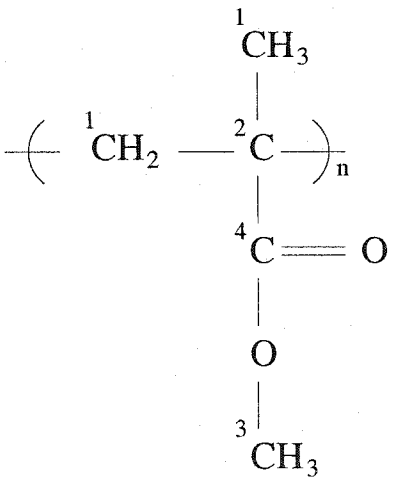

Figure 5.7: Chemical structure of PMMA

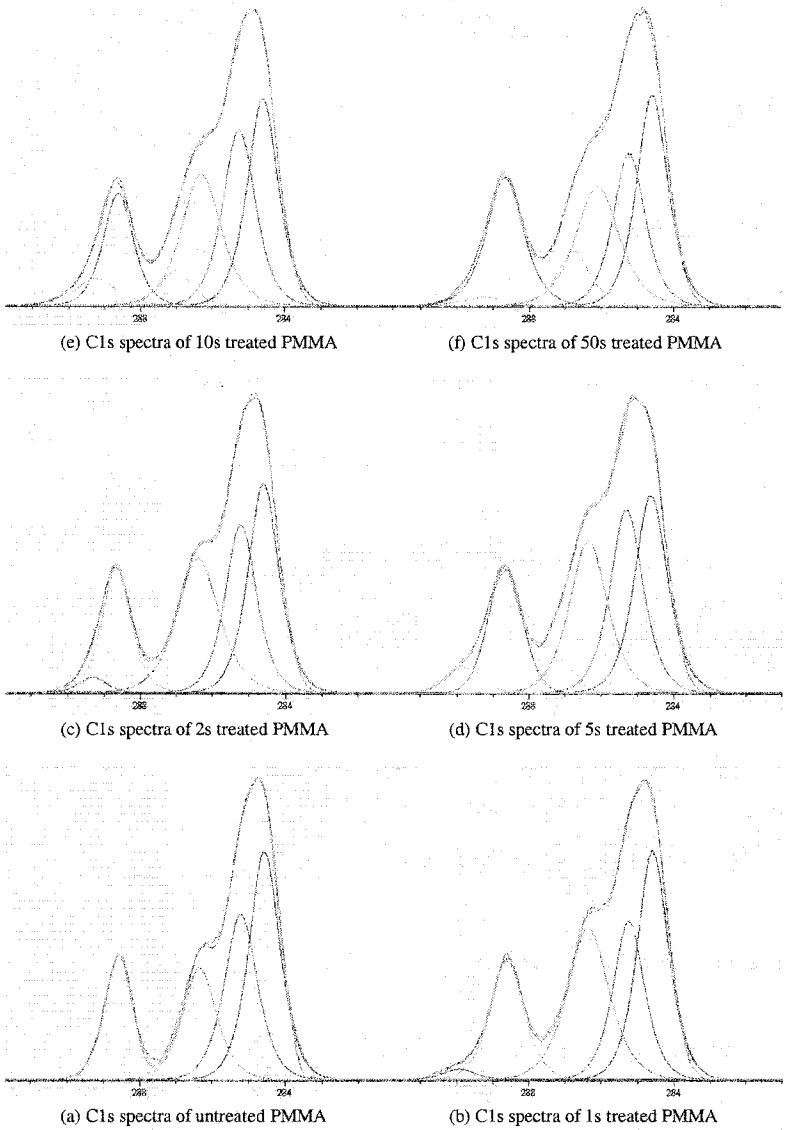

Figure 5.8: C 1s XPS spectra of plasma treated PMMA.

Table 5.4: Relative area of different components of C1s envelope for O_2 plasma treated PMMA

Treatment (s)	C1s (1) (%)	C1s (2) (%)	C1s (3) (%)	C1s (4) (%)	C1s (5) (%)	C1s(6) (%)
0	35.43	27.53	19.42	17.63	0	0
1	31.12	21.91	27.88	17.54	1.51	0
2	30.03	24.47	26.76	16.90	1.85	0
5	26.86	24.97	23.85	16.82	3.52	3.98
10	27.98	24.64	23.02	14.71	4.87	4.77
50	27.87	20.74	22.03	20.29	1.46	7.61

289.8 eV, corresponds to carbonate groups $O_2C{=}O$; and C1s (6), located at 287.2 eV, is attributed to free carbonyl groups C=O (Fig. 5.8). The percentages of different bonding contributions, estimated from the ratios of the peak area of Fig. 5.8, are given in Table 5.4. It can be seen that the component C1s (3) increases rapidly from 19.42% at 0 s to 27.88% at 1 s and then decreases slowly. The C1s (4) component decreases slowly from 17.63% to 14.71% upon a 10 s exposure, but increases to 20.29% for a 50 s treatment. Starting with 1.51% for a 1 s plasma treatment, the component C1s (5) increases to 4.87% (10 s) with a concomitant decrease in the C1s (3) and C1s (4) components, and then decreases to 1.46% at 50 s treatment. Upon a 5 s plasma exposure, the C1s (6) component becomes apparent and continuously increases to 7.61 % for a 50 s exposure. Thus, the first stage of surface modification could be the increase of C1s (3), and then the formation of C1s (5) and C1s (6). However, it is difficult to assure whether the formation of C1s (5) and C1s (6) are due to breakdown of C1s (3) and C1s (4) or to independent occurrence.

Overall, the calculated oxygen contents (in percentage) of the plasma modified

PMMA surfaces as a function of discharge exposure time are presented in Fig. 5.9. It can be seen that the surface chemical compositons are very sensitive to the treatment time. The main effects of modification occur during the first five seconds of the treatment; the percentage of O then increases slowly with time.

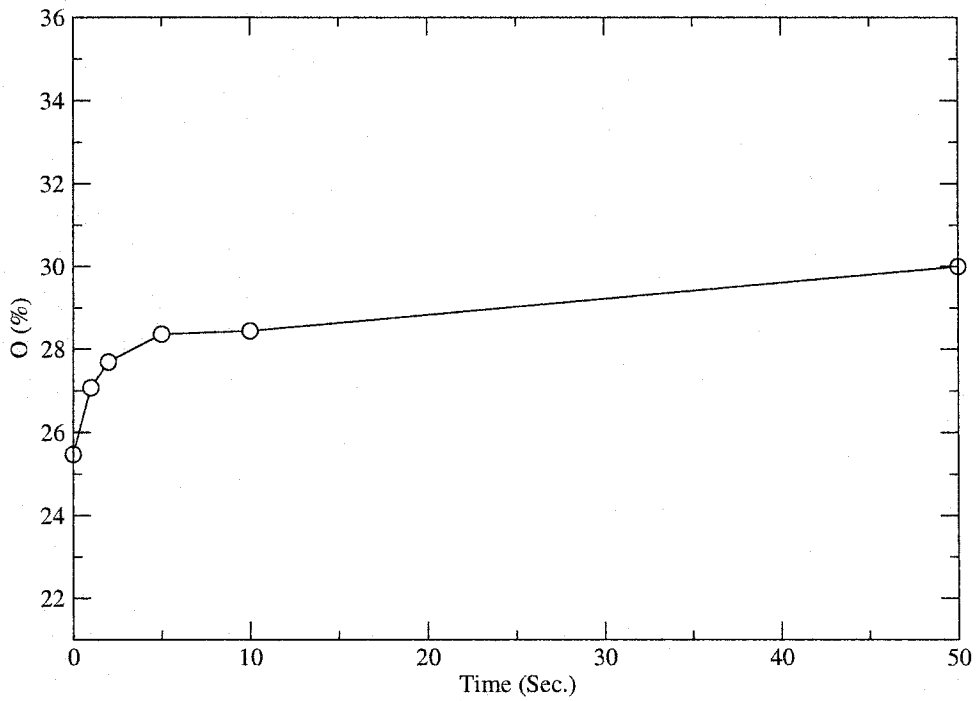

Figure 5.9: Oxygen percentage of PMMA after exposure to plasma.

5.3.4 Surface Topography

In this experiment, an optical profilometer is employed to profile the surface topography of modified PMMA films. Particularly, the surface roughness will be quantitatively determined by the high sensitivity of profilometer in vertical profiling.

Figure. 5.10 demonstrates the image of PMMA surfaces before and after plasma treatment. We found that the untreated PMMA film prepared by a spin-coating method is very smooth and has a root mean square (rms) roughness of 6 nm. The roughness of the surfaces did not increase appreciably up to a 10 s plasma treatment. The rms average of the measured height deviation increases to 16 nm upon a 50 s treatment. It is apparent that prolong treatment time will result in an increased etching effect via oxygen plasma, leading to a roughened spongy-like surface.

5.4 Discussion

The wettability improvement of PMMA surface by plasma treatment as well as other polymers has been reported in the literature from earliest studies dealing with plasma modification [56]. This enhancement is caused by the increase in surface free energy. So far, how plasma-treatment changes the surface energy of polymer surface is not completely understood. Most work related the wettability change to the incorporation of oxygen species by plasma activation [57, 58, 59].

The activation mechanism is believed to be the creation of free radicals on the polymeric material's surface molecules and then subsequent coupling of these free radicals with active species from the oxygen plasma environment [9]. In the case of a DC pulsed plasma condition set for our experiments, the effective glow duration time

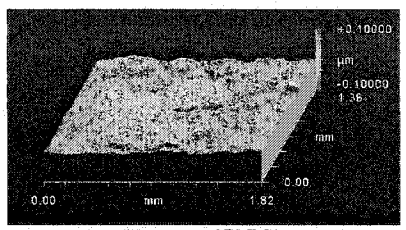

(a) untreated PMMA

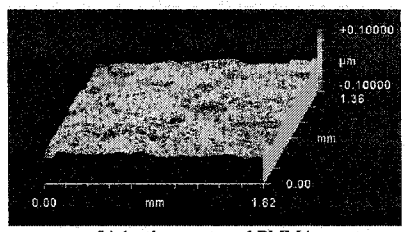

(b) 1s plasma treated PMMA

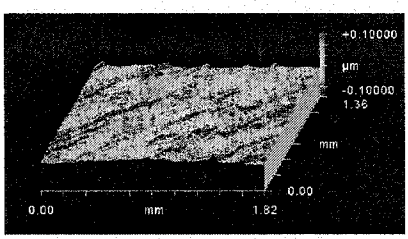

(c) 10s plasma treated PMMA

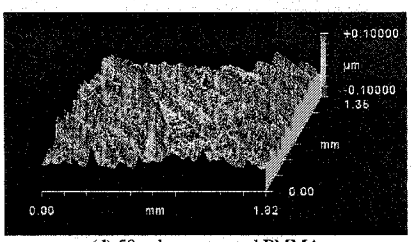

(d) 50s plasma treated PMMA

Figure 5.10: Surface topography of untreated and plasma treated PMMA

is very short, when compare to the effective afterglow duration time on account of the low pulse width and frequency. Thus, the long life singlet state molecular $O_2(^1\Delta)$ and the atomic species in ground state $O(^3P)$ are expected to be reactive with the PMMA surface [60, 61]. First, hydrogen is abstracted from the C–H bond in PMMA by atomic oxygen, yielding a free radical site such as:

$$\text{R–CH}_2\text{–R'} + \text{O}(^3\text{P}) \rightarrow \text{R–}\dot{\text{C}}\text{H–R'} + \dot{\text{O}}\text{H}$$

Then, these free radicals are likely to react with singlet state molecular oxygen $O_2(^1\Delta)$ to create a peroxy radical:

$$\text{R–}\dot{\text{C}}\text{H–R'} + \text{O}_2(^1\Delta) \rightarrow \text{R–CHO}\dot{\text{O}}\text{–R'}$$

These peroxyradicals are stabilized by hydrogen transfer (from the same or a neighboring chain) to form a hydroperoxide and a new radical site. There is a multiplicity of oxidation mechanisms that can be proposed in PMMA since there are at least three potential sites for initiating the oxidation reaction by a C–H bond rupture and different oxidative reactions that take place simultaneously while competing with each other. Figure. 5.11 presents the oxidation schemes for the formation of carboxyl, carbonyl and carbonate groups.

It is true that the plasma modified surface will become hydrophilic due to the incorporation of polar functional groups on account of the propensity of water molecules to form hydrogen bonds. However, the change of surface energy can be ascribed to

many other effects such as surface charge and roughness, in addition to chemical structure. Coen et al. reported the creation of a conductive surface layer on polymers by low-pressure plasma treatments [62]; while Gil'man et al. related the charge density variation to the wettability of plasma modified polymer surfaces [63]. Nevertheless, the zeta potential effect on solid surface tension of polymeric materials after plasma treatment remains unclear in literature. From Figures. 5.3 and 5.4, we observed an obvious relationship between zeta potential and contact angle of water on O_2 plasma treated PMMA.

The origins of interfacial charges are believed to come from the following various mechanisms [39, 53]:

1. Ionization of surface group,
2. Differential dissolution of ions from surfaces of sparingly soluble crystals,
3. Isomorphic substitution,
4. Charged crystal surface, and
5. Specific ion adsorption.

In this study, the increase in charges of modified PMMA surfaces in water can come about in two ways [64]: (1) by the generation of charge states due to plasma treatment and (2) by the ionization or dissociation of created new functional groups (e.g., the dissociation of protons from surface carboxylic groups [$-COOH \rightarrow -COO^- + H^+$]). Both of them lead to a negatively charged surface and the final surface charge is

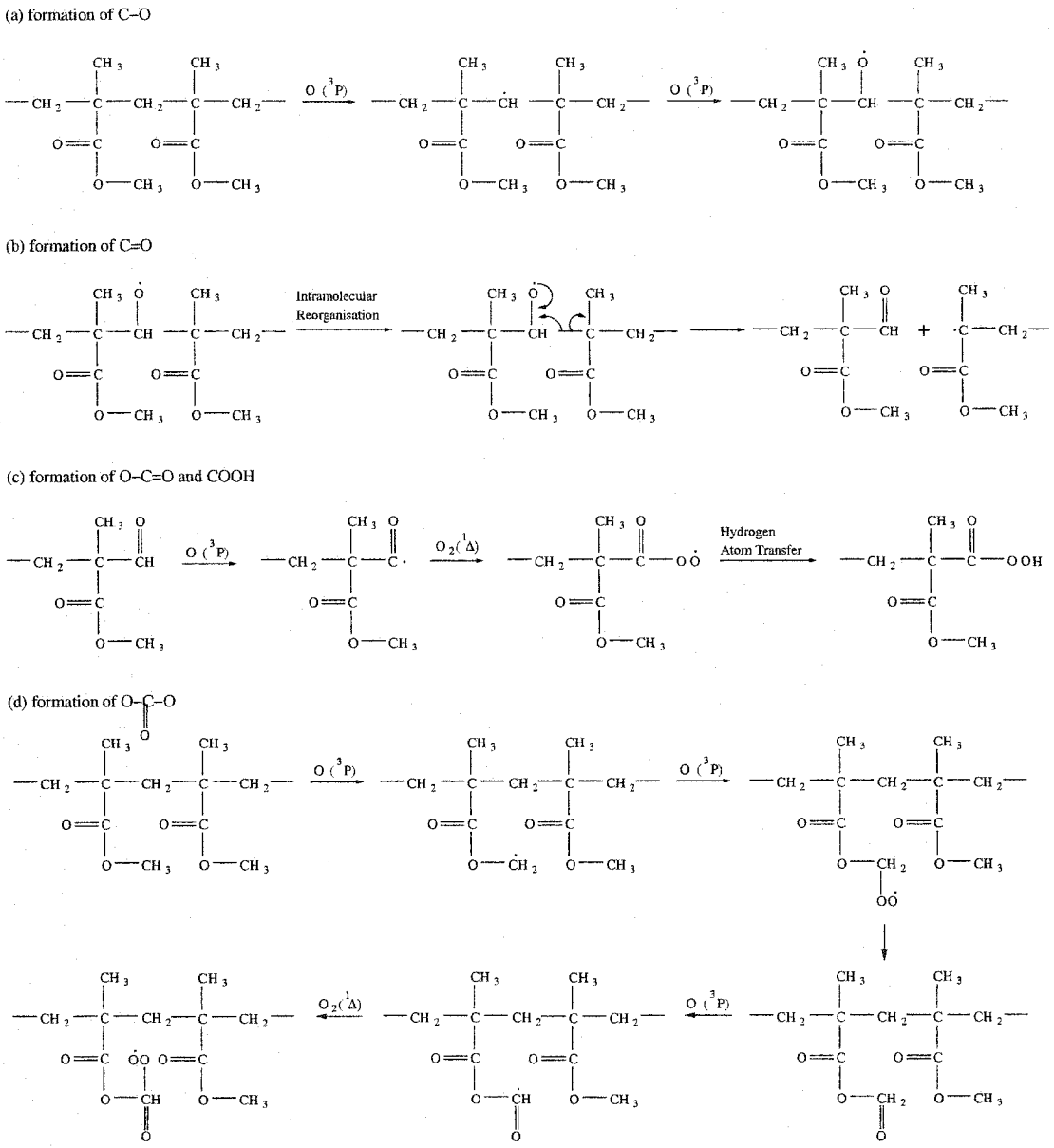

Figure 5.11: Oxidation scheme of O_2 plasma treated PMMA.

balanced by an equal but oppositely charged atmosphere of counterions in rapid thermal motion near the surface, leading to a stronger electrical double layer (EDL).

When a water droplet is in contact with a solid surface, the droplet will spread until a free energy minimum is reached and is determined by the interaction between the liquid and surface. When the surface has a zeta potential ζ, a charge density σ builds up in the EDL of the liquid phase, causing the solid-liquid interfacial tension to be different from that without EDL. Using Lippmann's equation, a solid-liquid interfacial tension contributed by the EDL effect γ_{sl}^{EDL} can be taken as [53]

$$\gamma_{EDL} = \frac{dU}{dA} = \int \sigma d\psi \tag{5.14}$$

where σ and ψ are surface charge density and surface potential in the EDL, respectively. After inserting the charge density from Eq. (5.13) and integrating Eq. (5.14) from $\psi = 0$ to $\psi = \zeta$, γ_{sl}^{EDL} can be given by

$$\gamma_{sl}^{EDL} = \frac{8n_{\infty}kT}{\kappa}(\cosh\frac{e\zeta}{2kT} - 1) \tag{5.15}$$

Thus, in the presence of an EDL effect, γ_{sl} as it appears in Young's equation (4.1) should be written as

$$\gamma_{sl} = \gamma_{sl}^{0} - \gamma_{sl}^{EDL} \tag{5.16}$$

where γ_{sl}^{0} and γ_{sl} are the solid-liquid interfacial tensions without and with EDL effect, respectively. Hence, a modified Young's equation can be written as

$$\gamma_{lv}\cos\theta_Y = \gamma_{sv} - (\gamma_{sl}^{0} - \gamma_{sl}^{EDL}) \tag{5.17}$$

It is now instructive to rewrite the equation of state approach Eq. (5.2) as

$$\gamma_{sl}^{0} = \gamma_{lv} + \gamma_{sv} - 2\sqrt{\gamma_{lv}\gamma_{sv}}(1 - \beta(\gamma_{lv} - \gamma_{sv})^2) \tag{5.18}$$

The use of γ_{sl}^{0} instead of γ_{sl} represents the fact that the equation of state relation did not consider any additional (unexpected) effect on the solid-liquid interfacial tension such as that due to EDL interactions. Combining Eq. (5.18) with the modified Young's equation (5.17) yields

$$\gamma_{lv}(1 + \cos\theta_Y) - \gamma_{sl}^{EDL} = 2\sqrt{\gamma_{lv}\gamma_{sv}}(1 - \beta(\gamma_{lv} - \gamma_{sv})^2) \tag{5.19}$$

As γ_{sl}^{EDL} can be determined from Eq. (5.15) by means of the experimental ζ potential values in Figure 5.4, the γ_{sv} value for each solid-liquid pair with known γ_{lv} and θ can be calculated from the above equation of state Eq. (5.19). Once γ_{sv} is known, the values of γ_{sl}^{0} can be determined by means of either Eq. (5.17) or (5.18). The computed $\gamma_{lv}\cos\theta$, γ_{sv}, γ_{sl}^{0}, γ_{sl}^{EDL}, γ_{sl} and their variations using those at zero time as references are shown in Table 5.5. Direct comparison of the values of γ_{sl} between Tables 5.1 and 5.5 indicates that the assumption used in the equation of state approach in neglecting EDL effect on contact angles is reasonable as the contribution of EDL effect to the solid-liquid interfacial tension γ_{sl}^{EDL} is extremely small, causing nearly no variation in the calculated γ_{sv} and γ_{sl} values, at least for the systems considered here. We conclude that it is not the EDL that makes the plasma-modified PMMA surfaces hydrophilic; rather, the main contribution of hydrophilicity results from the variation of the total surface tensions γ_{sv} and γ_{sl}.

It should be mentioned that surface roughness may also affect the wettability

Table 5.5: Calculated $\gamma_{lv}\cos\theta$, γ_{sv}, γ_{sl}^{0}, γ_{sl}^{EDL} and γ_{sl} for various PMMA surfaces with different plasma treatment times. Their variations in reference to the respective zero time ($t = 0$ s) values are also shown.

Treatment (sec)	$\gamma_{lv}\cos\theta$ (mJ/m^2)	γ_{sv} (mJ/m^2)	γ_{sl}^{0} (mJ/m^2)	γ_{sl}^{EDL} (mJ/m^2)	γ_{sl} (mJ/m^2)
0	21.86	40.09065	18.23086	0.00153	18.22933
1	34.67	46.85026	12.16361	0.00279	12.16082
2	42.53	51.22101	8.70175	0.00716	8.69459
5	45.26	52.80551	7.55707	0.00837	7.54870
10	45.55	52.97995	7.43496	0.00910	7.42586
50	45.75	53.09609	7.35410	0.00960	7.34450
Treatment (sec)	$\Delta\gamma_{lv}\cos\theta$ (mJ/m^2)	$\Delta\gamma_{sv}$ (mJ/m^2)	$\Delta\gamma_{sl}^{0}$ (mJ/m^2)	$\Delta\gamma_{sl}^{EDL}$ (mJ/m^2)	$\Delta\gamma_{sl}$ (mJ/m^2)
0	0	0	0	0	0
1	12.81	6.75961	−6.06725	0.00126	−6.06851
2	20.67	11.13036	−9.52911	0.00563	−9.53474
5	23.40	12.71486	−10.67379	0.00684	−10.68063
10	23.69	12.88930	−10.79590	0.00757	−10.80347
50	23.80	13.00554	−10.87676	0.00807	−10.88483

of surfaces. On very rough surfaces, contact angles are generally larger than those on smooth and chemically identical surfaces [33]. Based on the results of surface topography in Fig. 5.10, variation of 10 nm in roughness between the untreated PMMA and 50 s plasma treated PMMA substrate does not have a significant effect on the wettability: the contact angle remains nearly 51.0° as the treatment time changed from 10 to 50 s.

Chapter 6

Plasma-based surface patterning on SAMs

In this section, a set up of micro plasma discharge was developed for patterning surfaces in micron scale as an application of plasma-based surface modification. The substrates were prepared via self-assembled monolayers (SAMs) of alkanethiolates on gold films. Optical microscopy and SEM were employed to characterize the patterned surfaces.

6.1 Micro structure electrodes

In the booming research field of the miniaturization of analytical instruments and methods ("lab-on-the-chip") there is an increasing interest in plasma sources which can be operated on micro-chips. The plasmas have to be sufficiently powerful and robust when samples are introduced and they have to be sustained in very small volumes inside the chip without causing damage to the device. The miniaturized dimension and physical properties of micro plasma discharge make it suitable to fulfill this challenging task for the biotechnology, medicine and process analysis [65].

The main reason for using micro structure electrodes (MSE) or micro hollow cathode discharge (MHCD) is to enhance the electric field locally when a potential

difference is applied on the electrodes. Since the basic electrical discharge creation process in gases proceeds via electron impact ionization, electrons must be accelerated by the applied field E over the mean free path λ to gain a minimum kinetic energy [66]:

$$E_{kin} = eE\lambda > E_{ex} \tag{6.1}$$

where E_{ex} is the threshold energy necessary for electron excitation, dissociation, fragmentation or ionization of the gas. Therefore, operation of electrical discharge devices requires either a low gas pressure, i.e. large λ, or a very strong electric field $E = U/d$. Micro structure electrodes can provide distances on a micro-scale between the electrode elements. Thus, even at moderate voltages, the electrostatic field can exceed the threshold value required to initiate the electrical breakdown process. In this regard, it is also possible to produce electrical gas discharges up to near atmospheric pressure by means of MSE with very moderate voltages so that a wide area of plasma applications becomes feasible under reasonable conditions. The microdimensions of the discharge combined with convenient plasma parameters make it very attractive for MEMS and lab-on-a-chip applications.

Normally the MSE or MHCD is a multilayer system consisting of two metallic foils (Cu, Ni, Pt or W) separated by an insulator (polymer, mica, glass or ceramic). The thickness of the layers is typically $30 - 150$ μm. A hole with a diameter varying from tens to hundreds of μm is drilled through the structure. The MSE-sustained discharge can be considered as a normal glow discharge whereby the excitation and ionization efficiency is increased by the specific hollow cathode configuration [67]. Applying direct current (DC) or alternative current (AC), a weakly ionized plasma

is produced inside the hole between the electrodes. The operation of the discharge depends mainly on the ratio between the hole diameter and the distance between the electrodes, the gas pressure and current density. A very high density of electrons and metastable atoms is generated in the discharge due to the hollow cathode geometry. The reduced dimensions of the electrodes enable high pressure operation according to the laws of similarity [68]. The discharge can be operated in the pressure range from $\sim$ 10 Torr to 1 Atm.

6.2 Material preparation

A recent advance in the fabrication of nanoscale coatings is the use of the so-called Self-Assembled Monolayers (SAMs) [69, 70, 71, 72]. These films are two-dimensional organic assemblies that form spontaneously by chemisorption and self-organization of functionalized, long-chain organic molecules onto the surfaces of appropriate substrates. They provide models to systematically study a wide range of interface/surface phenomena. The organic and biological properties of these films are largely controlled by the end groups of the molecules and can be manipulated by tailoring the end functional groups. A schematic of SAMs is shown in Fig. 6.1. SAMs are of technical interest for the fabrication of sensors, protective layers, lubrication, and as patternable materials. They provide a pathway for a better understanding of many technological systems where interfacial events play a dominant role.

Among various types of SAMs, the best characterized systems are alkanethiolates (carbon chains with a sulfur atom at one end) on gold [73]. The formation principle is simple: A molecule which is essentially an alkane chain, typically with 10-20

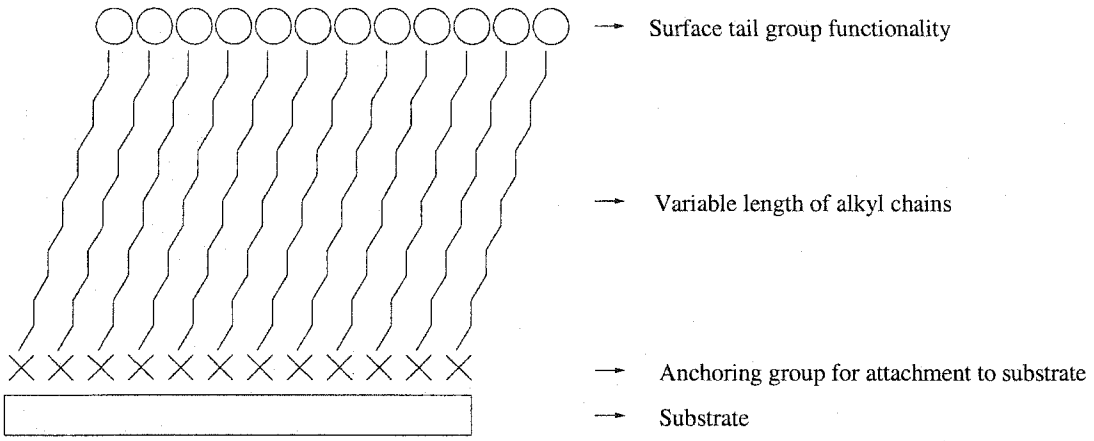

Figure 6.1: Schematic illustration of a self-assembled organic monolayer.

methylene units, is given a head group with a strong preferential adsorption to the substrate used. Thiol (S-H) head groups and Au (111) substrates have been shown to work excellently. The thiol molecules adsorb readily from solution onto the gold, creating a dense monolayer with the tail group pointing outwards from the surface. By using thiol molecules with different tail groups, the resulting chemical surface functionality can be varied within wide limits. Alternatively, it is also possible to chemically functionalize the tail groups by performing reactions after assembly of the SAMs.

SAMs of alkanethiolates on gold exhibit many of the features that are most attractive about self-assembling systems: ease of preparation, density of defects low enough to be useful in many applications, good stability under ambient laboratory conditions, and amenability to control interfacial properties. By changing the terminal groups or the length of alkane chain, desired surface characteristics such as wettabil-

ity or adhesion can achieved on SAMs and this capability can be further exploited by patterning the surfaces with different chemical and physical properties in discrete regions with micrometer spatial resolution. This has motivated several groups to begin exploring methods for patterning SAM films including microcontact printing [74], photooxidation [75], photolithography [76], electron beam or ion-beam writing [77], micromaching [78] and microwriting [79], etc. Here, micro plasma discharge is suggested as an alternative approach to pattern the SAMs.

In this experiment, silicon wafers of test grade were obtained from Wafer World (West Palm Beach, FL) in circular discs of about 10 cm diameter and were cut into rectangular shapes of about 1 cm $\times$ 1 cm . Gold shot (99.999%) and titanium shot (99.995%) were obtained from Kurt J. Lesker (Clairton, PA). Ethanol (100%) was obtained from the Chemistry Dept. at University of Alberta. Octadecanethiol [$CH_3(CH_2)_{17}SH$] and 16-mercaptohexadecanoic acid [$HS(CH_2)_{15}COOH$] were obtained from Aldrich and used as received.

As the most common method, evaporation of Au onto a flat Si wafer is employed to prepare gold thin film. Since the level of adhesion between the deposited Au film and Si is weak, an interlayer of titanium was used to enhance the adhesion. Au/Ti/Si substrates were prepared by sequentially evaporating $\sim$ 100 Å Ti and $\sim$ 1000 Å Au onto small rectangular Si wafers in a diffusion-pumped vacuum chamber at a rate of $\leq$ 2 Å/s under a pressure of 2 $\times$ 10^{-6} Torr. Au prepared by evaporation at room temperature is typically polycrystalline and has a predominately (111) structure, which is closely packed, three-fold symmetric. Once Au(111) substrate is immersed into thiol solutions, the thiol atoms adsorb directly on a 3-fold hollow site. This is

the lowest energy adsorption site of thiol onto Au(111) [80, 81, 82].

The evaporated Au surfaces were rinsed with ethanol before SAMs formation. Since organic contaminants are easily adsorbed onto high energy Au surfaces, evaporated gold surfaces were also flame annealed for $\sim$ 30 s using a bunsen burner under ambient laboratory condition in order to remove most organic contaminants. After $\sim$ 1 minute, the annealed substrates were then immersed into 1 mM of alkanethiolates in ethanol overnight.

6.3 Experimental

6.3.1 Experimental setup

In this study, Pyralux ® AP (Dupont, PA, cat# AP9222R) was used as the material of MSE device. This double-sided, copper-clad laminate is an all-polyimide composite of polyimide film bonded to copper foil. The inner 70 μm polyimide film serves as the dielectric and 70 μm double-sided copper foil acts as both cathode and anode. Polyimide was chosen as the dielectric because of its electrical and mechanical properties as well as its excellent thermostability. The laminates were cut into circular shapes of about 30 mm in diameter and the microdischarge cavities, $\sim$ 200 μm in diameter, were mechanically drilled through the three layer structure with a total thickness of 210 μm. Once fabricated, the MSE device was connected to a DC pulsed power as a micro plasma reactor and was fixed inside the vacuum chamber by a Teflon holder. The substrates of SAMs were mounted on a XYZ translation stage purchased from Oriel Spectra-Physics. Thus, the motion of the sample can be controlled in three dimension with sub-micrometer resolution and only the required area of the surface

will be exposed to the microdischarge. A schematic view of the experimental set-up is presented in Fig. 6.2.

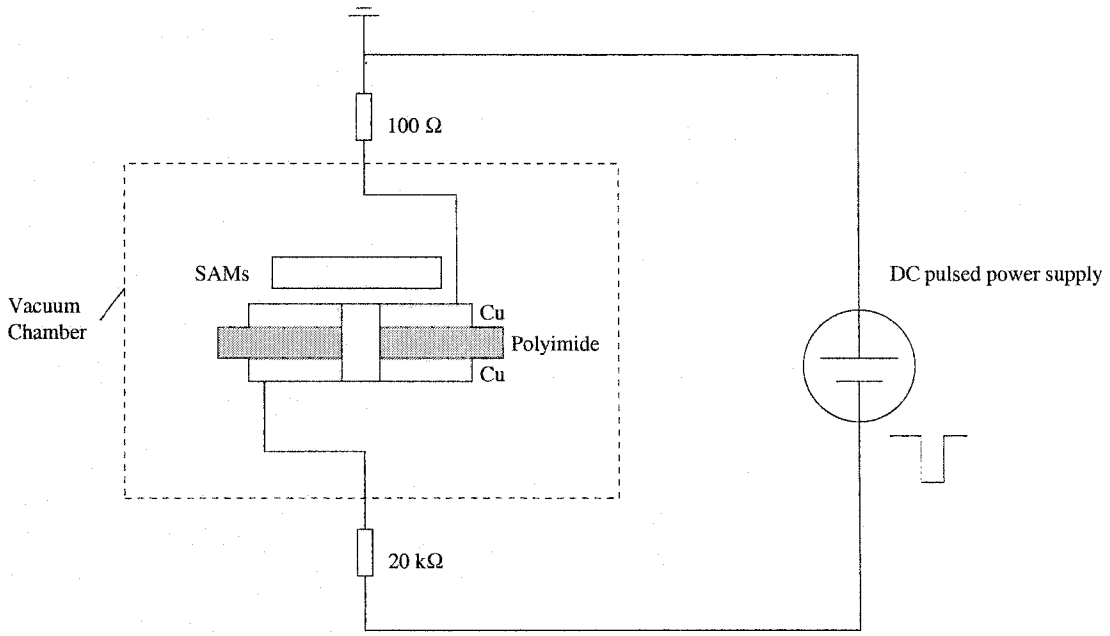

Figure 6.2: Schematic of the microdischarge experimental set-up.

6.3.2 Patterning procedures

The patterning procedures are summarized in Fig. 6.3. The first step has been described in the Material preparation section. A hydrophobic SAM was formed by reaction of an Au film with Octadecanethiol [$CH_3(CH_2)_{17}SH$]. The nonpolar CH_3 tail group makes the surface hydrophobic with a water contact angle of 118° [83].

The second step of patterning procedure involves micro plasma exposure of Ar to SAMs while the sample is moved by the translation stage to produce line-shaped bare gold region. During this step, negative DC pulses of 100 Hz frequency were

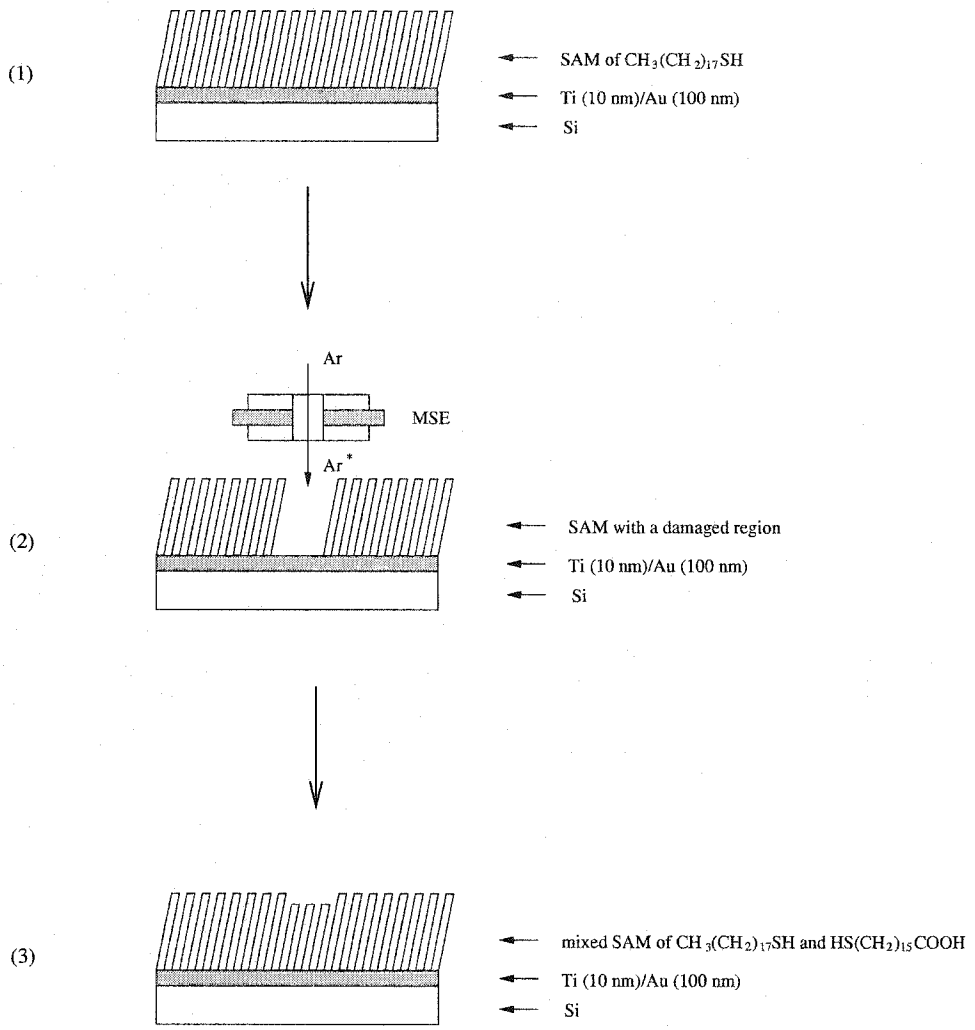

Figure 6.3: Schematic of patterning procedure by micro plasma discharge. (1) A SAM formed from octadecanethiol on a 100 nm Au film supported by a Si wafer; (2) The sample was exposed to the metastable Ar atoms through MSE plasma, uncovering bare Au underneath the damaged alkanethiol region; (3) The treated sample was immersed in a 1 mM ethanolic solution of 16-mercaptohexadecanoic acid. The adsorbates in the damaged region were displaced by the carboxylic acid terminated thiol.

delivered to the cathode of the micro structure electrode to generate glow discharge in Ar at a pressure of 10 Torr. Facing towards the anode, the SAMs samples were moved by the translator at a speed of 200 μm/s to be exposed to the excited Ar atoms, resulting in a 1 cm straight line of bare gold. In order to ensure a minimum line width corresponding to the cavity dimension of the MSE, the power density and pulse width were adjusted to 1.5 kV and 5 μs by the Velonex 360 high power pulse generator and the V-I signals were monitored by a Tetronix digital osilloscope (TDS3014B).

Third, a second hydrophilic SAM was formed selectively on the bare gold region by immersion of the plasma treated surface into a solution of 16-mercaptohexadecanoic acid [$HS(CH_2)_{15}COOH$]. The adsorbates in the damaged regions of the SAM were displaced by the carboxylic acid terminated thiol to form a wetting line. Thus, a patterned surface was produced with combined hydrophobic and hydrophilic neighboring regions.

6.4 Results and discussion

The ability to damage SAMs with metastable inert gas atoms was reported by the group of G. M. Whitesides [84, 85]. The mechanism by which organic molecules are damaged by metastable atoms has been studied and appears to involve a Penning ionization process [86]. In this experiment, the DC pulsed generator was used at a frequency ν of 100 Hz and a pulse duration time τ of 5 μs. The duty factor C_r can be obtained at 0.05 %. This verifies that the pulse-on discharge period is extremely short compared to the pulse-off period. Hence, the effect of electrons and positive

ions can be safely neglected and the damage to the SAMs can be considered to be mainly ascribed to metastable Ar atoms due to their longer lifetime and high density produced by the micro structure electrodes.

The different wetting properties of the neighboring regions on patterned SAMs can be observed by noting that liquid tends to spread on the hydrophilic lines. The fluidic line can be created by placing a small drop of water from a syringe on the sample surface and drawing the drop along the hydrophilic line. Figure. 6.4 shows the image of the patterned SAMs surface before the evaporation of the water drop by an optical microscope. The line width of about 200 μm for a 16-mercaptohexadecanoic acid monolayer was measured using the image of the fluidic line under a light microscope, which is comparable to the dimension of the hole drilled through the micro structure electrodes (Fig. 6.5).

It was observed experimentally that a wetting line can be formed on the argon plasma treated SAMs substrates either before or after immersing into the solution of 16-mercaptohexadecanoic acid. This implies that the Ar plasma has sufficiently uncovered the bare gold by taking both CH_3 terminal group and CH_2 backbone away from the surface, as both functional groups, if they expose on the surface, are hydrophobic. A more detail investigation on this subject would require the use of FTIR (Fourier Transform Infrared) Spectroscopic Microscope.

The width of the line and existence of different SAMs regions were also verified by scanning electron microscopy (SEM) in Fig. 6.6. When a nonconductive specimen is directly illuminated with an electron beam. Its electrons with a negative charge collected locally to cause specimen charge up, thus preventing normal emission of

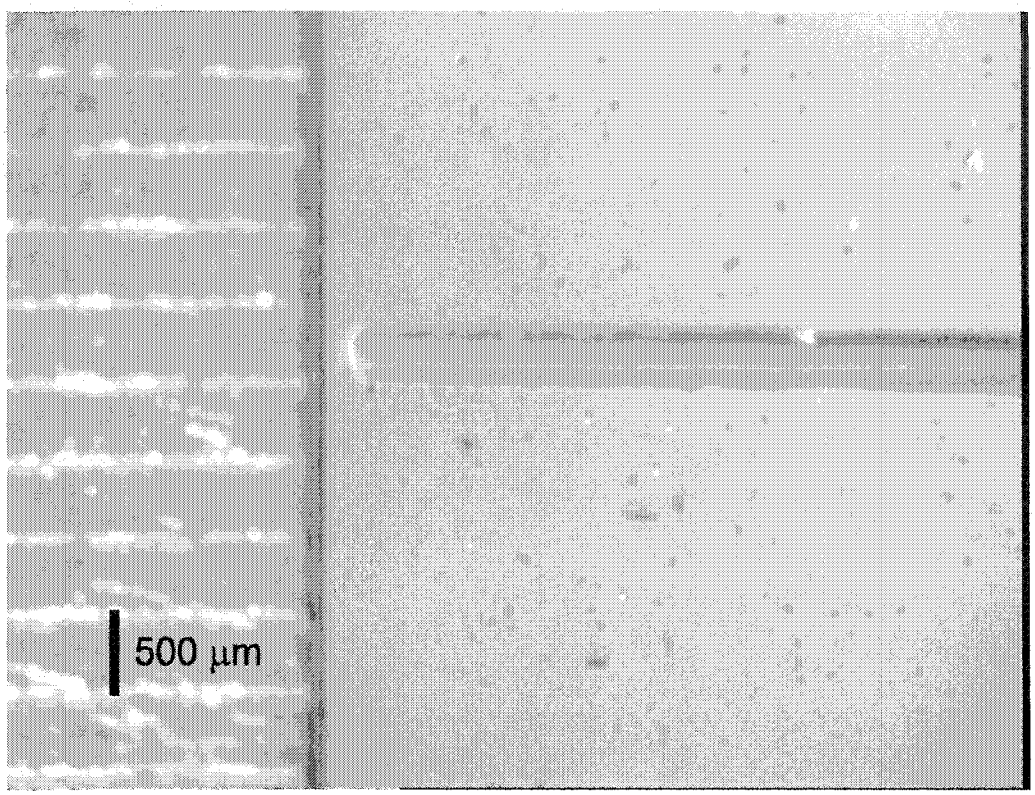

Figure 6.4: Optical micrograph of patterned SAM surface: the fluidic line represents the region of SAMs derived from $HS(CH_2)_{15}COOH$, while the region of background was derived from $CH_3(CH_2)_{17}SH$.

secondary electrons. Generally, lowering the accelerating voltage is used to reduce specimen charge up. Hence, a low electron beam voltage of 3.5 kV was applied for the SAMs imaging.

In SAMs of alkanethiolates on Au, most of the secondary electrons emitted by the sample originate from the gold. Images may arise by scattering of these electrons through the different components of SAMs, or by modulation of the surface potential by SAMs [87]. Material contrast in SEM occurs because different materials have differ-

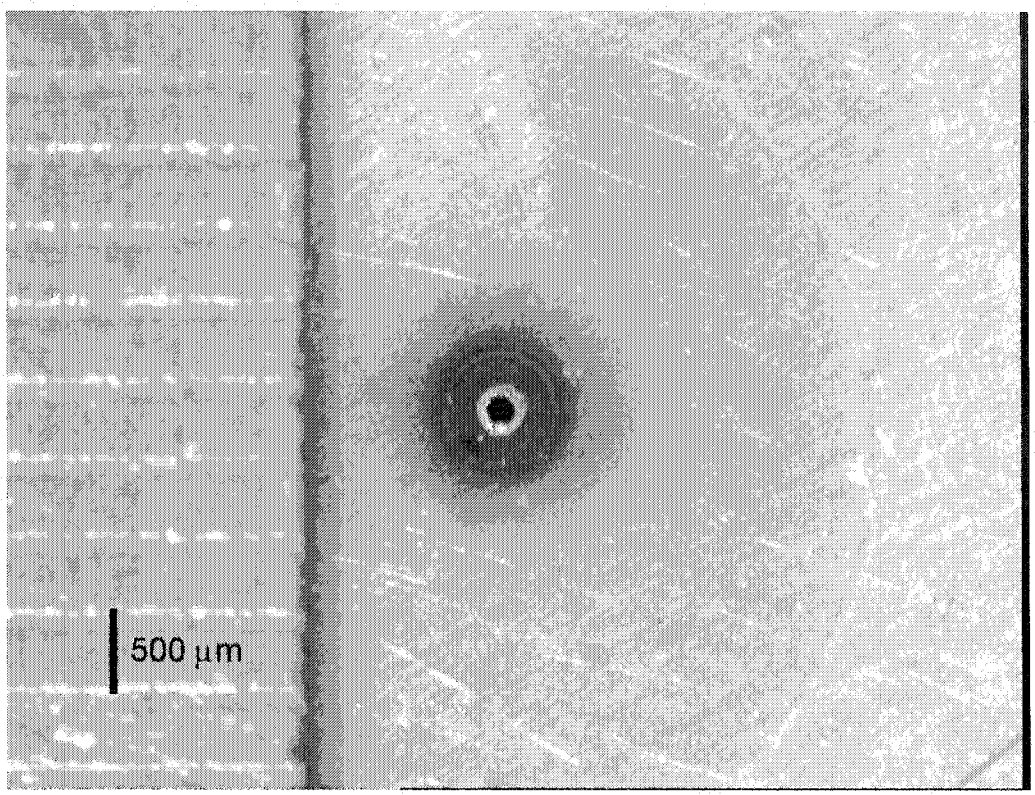

Figure 6.5: Dimension of MSE hole by optical microscope: each grid of scale is 500 μm.

ent secondary electron yields (δ) under primary electron bombardment. The contrast of brightness between neighboring regions of the patterned surface can be related to the different electron density of the functional groups in SAMs. It was found that increasing the concentration of atomic number Z of the functional group leads to an increase in the electron density in the SAMs and, as a result, in the increased scattering of secondary electrons emitted during SEM measurements [51]. Thus, increasing the average Z of heteroatoms in the tail functional groups from $CH_3(CH_2)_{17}SH$ to

$HS(CH_2)_{15}COOH$ results in a decrease in the brightness. In addition, contaminants adsorbed on regions of different interfacial free energy can also influence the image brightness as well. The $Au/HS(CH_2)_{15}COOH$ is darker than $Au/CH_3(CH_2)_{17}SH$ also due to a higher solid-vapor interfacial free energy for the former.

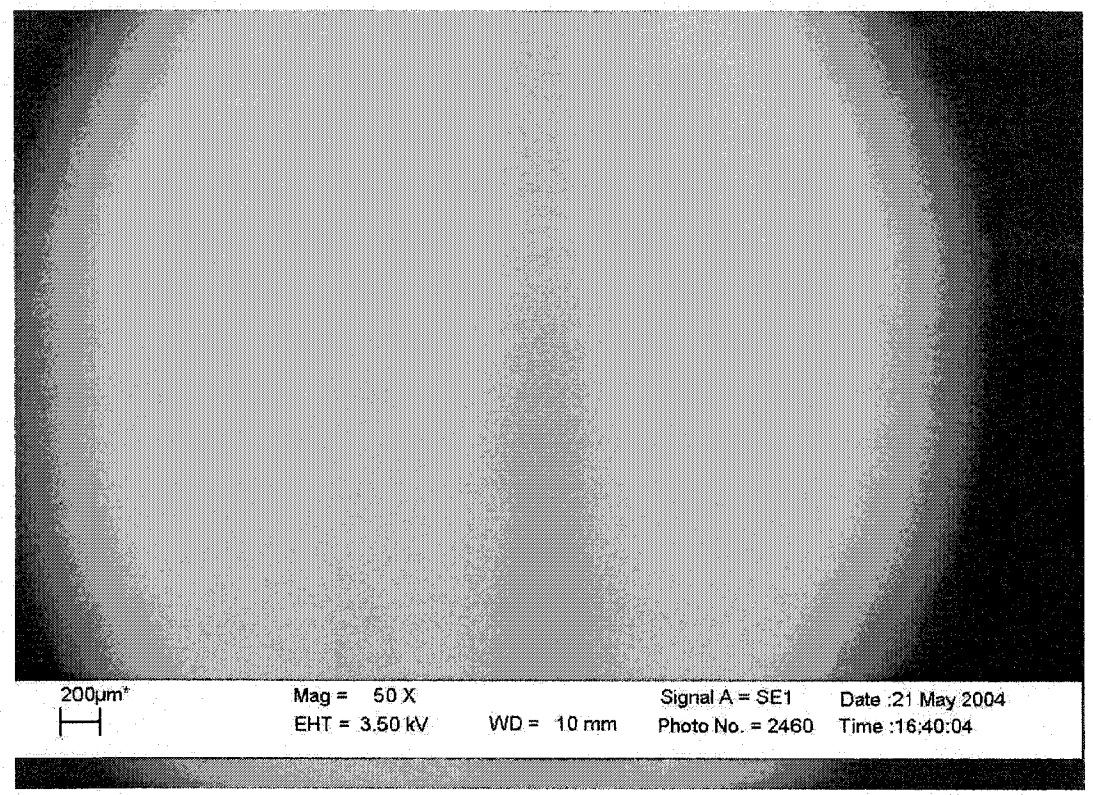

Figure 6.6: A SEM image of a patterned SAMs surface. Dark region: $Au/HS(CH_2)_{15}COOH$; bright region: $Au/CH_3(CH_2)_{17}SH$

The images from the optical microscope and SEM demonstrate the effectiveness of the application of micro plasma discharge for patterning alkanethiols on gold. The ability to damage SAMs with active plasma particles and to transform this damage

into other permanent structures may be useful to etch the patterned Au substrates in lithography. This method is noncontact and flexible since it provides convenient access to small features without using multiple lithographic steps associating with mask alignments. The desired pattern can be formed by the relative movement between the MSE and the treated sample. The spatial resolution in the present experiments can be improved by reducing the size of the cavity of MSE. By inserting molecules with contrasting chemical functional groups in the plasma treated regions of the SAMs, it allows creation of a lithographic resist by deposition of a thin polymeric layer in the patterned area [85]. Hence, this approach has the potential to produce the more complex patterns and can be extended to other systems such as SAMs on silicon wafers or polymeric substrates.

Chapter 7

Conclusions and Future Research

7.1 Conclusions

In an effort to study the fundamentals of plasma processing of organic materials, a set up of DC pulsed cold plasma discharge was established in this work. The surface modification of PMMA by oxygen plasma has been investigated with focus on the understanding of wettability change. Various surface analysis tools were employed to characterize the surface properties after plasma treatment and their influence on the solid surface tension were discussed. A novel method has been developed to pattern self-assembled monolayers with micro plasma discharge as an application of plasma surface modification. The results of the current project are summarized as the following:

1. The surfaces of PMMA were modified by means of a DC pulsed oxygen plasma. Polar functional groups such as carbonyl and carbonate groups were introduced into PMMA and their presence were confirmed by XPS analysis. Consequently, the wettability of PMMA surfaces increases rapidly within the first 5 s plasma treatment and remaines nearly unchanged after prolong treatment up to 50 s;

2. It was also found that variation of the zeta potential of the plasma treated PMMA surfaces behaves similar to those of wettability. The increase in negative zeta potential and surface charge density suggest that charge state and dissociation of the polar functional groups were created on the surfaces when in contact with water and electrolyte solutions;

3. The plasma modification results correlated well with wettability, zeta potential and chemical structure of the treated PMMA. An additional surface tension term was introduced into Young's equation due to an electrical double layer (EDL) effect upon plasma treatment. It can be concluded that the increase in wettability of the treated PMMA is due to simultaneous effect of chemical modification (which increases the solid surface tension) and the increase in zeta potential (which decreases the solid-liquid interfacial tension);

4. Combination of micro plasma discharge with molecular self-assembly offers a versatile tool for manipulating the structure and properties of surfaces on desired regions with the advantages of flexibility, noncontact and ease of operation. By using argon through micro structure electrodes, a patterned line was produced at a width of microscale on the treated surface.

7.2 Future work

The micro plasma discharge in material processing has demonstrated great potential in surface patterning techniques. The feasibility of patterning process using argon plasma selective modification has been proven with our initial results on self-

assembled monolayers. There are several issues in need of a deeper investigation in order to improve the performance of the process and future application of micro plasma patterning:

1. It was found that the power density and treatment time can seriously affect the final width of the patterned regions. A systematic study of the influence from input plasma parameters on the patterned surfaces is required. FTIR (Fourier Transform Infrared) Spectroscopic Microscope and SIMS-TOF (Secondary Ion Mass Spectroscopy based on Time-of-Flight mass spectrometer) are expected to have the capability to investigate chemical structures with fine lateral resolution in the narrow patterned area;

2. The diameter of the hole for the micro structure electrodes is limited by the capability of mechanical drilling. This can be improved by laser micromachining [88] or by chemical etching of the insulation layer after photolithographic patterning of metal layers [89]. Thus, the dimension of the cavity in MSE and the width of the patterned region can be reduced to a submicron scale;

3. By means of a micro plasma configuration, the discharge gap can be scaled down to several microns and accordingly the working pressure could be increased up to atmospheric. Hence, the micro plasma discharge can offer high density of active species without the need of expensive vacuum equipment. However, the intrinsic properties of this plasma source might be different from the low pressure plasma. The study of physical properties such as optical appearance and the current-voltage characteristics could help to reveal the mechanisms for generating a

controllable, self-sustained discharge at moderate and high pressures;

4. Using different gas types and various substrate materials can achieve versatile chemical and physical properties of the patterned surfaces on desired regions. For instance, fluorocarbon plasma will lead to hydrophobic surfaces and exposing alkylthiolate self-assembled monolayers on gold to oxygen plasma through MSE might result in bonding of alkylsulfonates to Au [75]. Better understanding of interactions between the plasma and treated surfaces is expected by molecular dynamics simulations of plasma-surface chemistry;

5. Based on the findings that plasma modification can change the zeta potential of the material surfaces, the micro plasma patterning could be used in the fabrication of non-uniform microfluidic devices that are applicable to biosensor and biomedical engineering for generation of different surface charges on surfaces.

"I was like a boy playing on the sea-shore, and diverting myself in now and then finding a smoother pebble or a prettier shell than ordinary, whilst the great ocean of truth lay all undiscovered before me."

–Isaac Newton

BIBLIOGRAPHY

[1] D. Hegemann, H. Brunner, and C. Oehr. Plasma treatment of polymers for surface and adhesion improvement. *Nuclear Instruments and Methods in Physics Research B*, 208:282, 2003.

[2] H. Lim, Y. Lee, S. Han, J. Cho, and K. J. Kim. Surface treatment and characterization of PMMA, PHEMA and PHPMA. *J. Vac. Sci. Technol. A*, 19(4):1490–1496, 2001.

[3] U. Schulz, P. Munzert, and N. Kaiser. Surface modification of PMMA by DC glow discharge and microwave plasma treatment for the improvement of coating adhesion. *Surf. & Coat. Technol.*, 142:507–511, 2001.

[4] H. Yasuda. Plasma for modification of polymers. *J. Macromol. Sci.*, A10(3):383–420, 1976.

[5] E. M. Liston, L. Martinu, and M. R. Wertheimer. Plasma surface modification of polymers for improved adhesion: a critical review. *J. Adhesion Sci. Technol.*, 7:1091–1127, 1993.

[6] C. Oehr. Plasma surface modification of polymers for biomedical use. *Nuclear Instruments and Methods in Physics Research B*, 208:40, 2003.

[7] D. C. Schram, T. H. J. Bisschops, G. M. W. Kroesen, and F. J. Hoog. Plasma surface modification and plasma chemistry. *Plasma Physics and Controlled Fusion*, 29(10A):1353–1364, 1987.

[8] F. D. Egitto and L. J. Matienzo. Plasma modification of polymer surfaces for adhesion improvement. *IBM J. Research & Development*, 38:423, 1994.

[9] D. M. Coates and S. L. Kaplan. Modification of polymeric material surfaces with plasmas. *MRS Bulletin*, Chapter IV, 1996.

[10] A. I. Drachev. Generation of polymer electrets in a low-temperature glow-discharge plasma. *High Energy Chemistry*, 37(5):297–302, 2003.

[11] D. J. Wilson, R. C. Pond, and R. L. Williams. Wettability of chemically modified polymers: experiment and theory. *Interface Sci.*, 8:389–399, 2000.

[12] I. Langmuir. The interaction of electron and positive ion space charges in cathode sheaths. *Phys. Rev.*, 33:954, 1929.

[13] A. Grill. *Cold plasma in materials fabrication.* IEEE Press, New York, 1993.

[14] M. A. Liebermann and A. J. Lichtenberg. *Principles of plasma discharges and materials processing.* Wiley, Mew York, 1994.

[15] I. B. Chapman. *Glow discharge processes.* Wiley, New York, 1980.

[16] H. Yasuda. *Plasma polymerization.* Academic Press, Orlando, 1985.

[17] A. A. Kurithof and F. M. Penning. Determination of the townsend ionization coefficient. *Physica*, 4:430–449, 1937.

[18] D. C. Gray, I. Tepermeister, and H. H. Sawin. Phenomenological modeling of ion-enhanced surface kinetics in fluorine-based plasma-etching. *J. Vac. Sci. & Technol.*, B11:1243–1257, 1993.

[19] M. Konuma. *Film deposition by plasma techniques.* Springer, New York, 1992.

[20] R. H. Hansen and H. Schonhorn. A new technique for preparing low surface energy polymers for adhesive bonding. *J. Polym. Sci. Polym. Lett. Ed.*, B4:203–209, 1966.

[21] H. Schonhorn, F. W. Ryan, and R. H. Hansen. Surface treatment of polypropylene for adhesive bonding. *J. Adhesion*, 2:93–99, 1970.

[22] D. T. Clark and A. Dilks. Esca applied to polymers. *J. Polym. Sci. Polym. Chem. Ed.*, 17:957–976, 1979.

[23] H. K. Yasuda, editor. *Plasma polymerization and plasma interactions with polymeric materials.* Wiley, New York, 1990.

[24] R. d'Agostino, editor. *Deposition, treatment and etching of polymers.* Academic Press, New York, 1990.

[25] R. Cormia. Use plasmas to reengineer your advanced materials. *Res. Dev. Mag.*, 32(7):60, 1990.

[26] L. M. Siperko and R. M. Thomas. Chemical and physical modification of fluoropolymer surfaces for adhesion enhancement - a review. *J. Adhesion Sci. Technol.*, 157:3, 1989.

[27] A. M. Howatson. *An Introduction to Gas Discharges.* Pergamon Press, Headington Hill Hall, 2 edition, 1965.

[28] J. S. Townsend. *Electricity in Gases.* Clarendon Press, Oxford, 1915.

[29] A. Bogaerts, E. Neyts, R. Gijbels, and J. Mullen. Gas discharge plasmas and their applications. *Spectrochimica Acta*, B57:609–658, 2002.

[30] R. Hugon, G. Henrion, and M. Fabry. Time resolved determination of the electron energy distribution function in a dc pulsed plasma. *Meas. Sci. Technol.*, 7:553–559, 1996.

[31] V. V. Ivanov, K. S. Klopovsky, D. V. Lopaev, Y. A. Mankelevich, A. T. Rakhimov, and T. V. Rakhimova. Structure and dynamics of a pulsed dc discharge in pure oxygen. *IEEE Trans. Plasma Sci.*, 31(4):528–541, 2003.

[32] T. A. Beer, J. Lamier, and H. Stori. Dynamics of a pulsed dc discharge used for plasma-assisted chemical vapor deposition. *Surf. & Coat. Technol.*, 120:331–336, 1999.

[33] D. Y. Kwok. Contact angle measurement and contact angle interpretation. *Adv. Colloid Interface Sci.*, 81:167–249, 1999.

[34] T. Young. An essay on the cohesion of fluids. *Philos. Trans. R. Soc. London*, 95:65, 1805.

[35] A. W. Neumann and J. K. Spelt, editors. *Applied surface thermodynamics.* Marcel Dekker Inc., New York, 1996.

[36] D. Y. Kwok, A. Leung, C. N. C. Lam, A. Li. R. Wu, and A. W. Neumann. Low-rate dynamic contact angles on poly(methyl methacrylate) and the determination of solid surface tensions. *J. Colloid Interface Sci.*, 206:44–51, 1998.

[37] Y. Rotenberg, L. Boruvka, and A. W. Neumann. Determination of surface tension and contact angle from the shapes of axisymmetric fluid interfaces. *J. Colloid Interface Sci.*, 93:169–183, 1983.

[38] P. Cheng, D. Li, L. Boruvka, and A. W. Neumann. Automation of axisymmetric drop shape-analysis for measurement of interfacial-tensions and contact angles. *Colloids Surf.*, 43:151–167, 1990.

[39] J. H. Masliyah. *Electrokinetic transport phenomena.* Alta, Edmonton, 1994.

[40] H. L. F. Helmholtz. Studies of electric boundary layers. *Wied. Ann.*, 7:337–382, 1879.

[41] G. Gouy. Constitution of the electric charge at the surface of an electrolyte. *J. Phys. Radium*, 9:457, 1910.

[42] D. L. Chapman. A contribution to the theory of the electrocapillarity. *Phil. Mag.*, 25:475, 1913.

[43] H. J. Jacobasch, F. Simon, and P. Weidenhammer. Adsorption of ions onto polymer surfaces and its influence on zeta potential and adhesion phenomena. *Colloid Polym. Sci.*, 276:434–442, 1998.

[44] F. Lu, J. Yang, and D. Y. Kwok. Numerical and experimental studies on electrical potential distribution of pressure-driven flow in parallel-plate microchannels. *J. Phys. Chem. B*, 2004. submitted.

[45] R. J. Hunter. *Zeta potential in colloid science: principles and applications.* Academic Press, San Diego, 3 edition, 1988.

[46] C. Werner, R. Zimmermann, and T. Kratzmüller. Streaming potential and streaming current measurements at planar solid/liquid surfaces for simultaneous determination of zeta potential and surface conductivity. *Colloids and Surfaces A*, 192:205–213, 2001.

[47] D. Briggs and M. P. Seah. *Practical Surface Analysis.* Wiley, Chichester, 1990.

[48] L. Reimer. *Scanning electron microscopy : physics of image formation and microanalysis.* Springer, New York, 1985.

[49] Y. Wu, K. Hayashi, N. Saito, H. Sugimura, and O. Takai. Imaging micropatterned organosilane self-assembled monolayers on silicon by means of scanning electron microscopy and kelvin probe force microscopy. *Surf. Interface Anal.*, 35:94–98, 2003.

[50] A. G. Bittermann, S. Jacobi, L. F. Chi, H. Fuchs, and R. Reichelt. Contrast studies on organic monolayers of different molecular packing in fesem and their correlation with sfm data. *Langmuir*, 17:1872–1877, 2001.

[51] G. P. Lopez, H. A. Biebuyck, and G. M. Whitesides. Scanning electron microscopy can form images of patterns in self-assembled monolayers. *Langmuir*, 9:1513–1516, 1993.

[52] P. J. Eaton, P. Graham, J. R. Smith, J. D. Smart, T. G. Nevell, and J. Tsibouklis. Mapping the surface heterogeneity of a polymer blend: an adhesion-force-distribution study using the atomic force microscope. *Langmuir*, 16:7887–7890, 2000.

[53] R. J. Hunter. *Foundations of colloid science.* Clarendon Press, Oxford, 1989.

[54] S. B. Amor, G. Baud, M. Jacquet, G. Nanse, P. Fioux, and M. Nardin. XPS characterisation of plasma-treated and alumina-coated PMMA. *Appl. Surf. Sci.*, 153:172–183, 2000.

[55] Kratos Analytical Co. High resolution XPS spectra of polymers. www.kratos.com, Manchester, 1997.

[56] D. Briggs, D. G. Rance, C. R. Kendall, and A. R. Blythe. Surface modification of poly(ethylene-terephthalate) by electrical-discharge treatment. *Polymer*, 21(8):895–900, 1980.

[57] P. Groning, M. C. Coen, and L. Schlapbach. Polymers and cold plasma. *Chimia*, 55(3):171–177, 2001.

[58] R. M. France and R. D. Short. Plasma treatment of polymers. *Faraday Trans.*, 93(17):3173–3178, 1997.

[59] B. Johansson, A. Larsson, A. Ocklind, and A. Ohrlund. Characterization of air plasma-treated polymer surfaces by esca and contact angle measurements for optimization of surface stability and cell growth. *J. Appl. Poly. Sci.*, 86:2618–2615, 2002.

[60] F. Clement, B. Held, N. Soulem, and C. Guimon. XPS analysis of polystyrene thin films treated under dc pulsed discharges conditions in nitrogen, oxygen and oxygen-argon mixtures. *Eur. Phys. J. AP*, 18:135–151, 2002.

[61] L. Lianos, D. Parrat, T. Q. Hoc, and T. M. Duc. Secondary-ion mass-spectrometry time-of-flight and in-situ x-ray photoelectron-spectroscopy studies of polymer surface modifications by a remote oxygen plasma treatment. *J. Vac. Sci. Technol. A*, 12(4):2491–2498, 1994.

[62] M. C. Coen, P. Groening, G. Dietler, and L. Schlapbach. Creation of a conductive surface layer on polypropylene samples by low-pressure plasma treatments. *J. Appl. Phys.*, 77(11):5695–5701, 1995.

[63] A. B. Gil'man, L. A. Rishina, A. I. Drachev, and L. S. Shibryaeva. Polypropylene films in a direct-current discharge. *High Energy Chemistry*, 35(2):151–156, 2001.

[64] J. N. Israelachvili. *Intermolecular and Surface Forces.* Academic Press, London, 1985.

[65] M. Miclea, K. Kunze, J. Franzke, and K. Niemax. Plasmas for lab-on-chip applications. *Spectrochimica Acta B.*, 57:1585–1592, 2002.

[66] K. H. Gericke, C. Geβner, and P. Scheffler. Microstructure electrodes as means of creating uniform discharges at atmospheric pressure. *Vacuum*, 65:291–297, 2002.

[67] C. Penache, M. Miclea, A. B. Bräuning-Demian, O. Hohn, S. Schossler, T. Jahnke, K. Niemax, and H. Schmidt-Böcking. Characterization of a high-pressure microdischarge using diode laser atomic absorption spectroscopy. *Plasma Source Sci. Technol.*, 11:476–483, 2002.

[68] A. von Engel. *Ionized gases.* Clarendon Press, Oxford, 1965.

[69] C. D. Bain and G. M. Whitesides. Modeling organic-surfaces with self-assembled monolayers. *Angew. Chem. Int. Ed.*, 28(4):509, 1989.

[70] G. M. Whitesides and P. E. Laibinis. Wet chemical approaches to the characterization of organic-surfaces-self-assembled monolayers, wetting, and the physical organic-chemistry of the solid liquid interface. *Langmuir*, 6:87, 1990.

[71] A. Ulman. *Introduction to thin organic films: from Langmuir-Blodgett to self-assembly.* Academic Press, Boston, 1991.

[72] L. H. Dubois and R. G. Nuzzo. Synthesis, structure, and properties of model organic-surfaces. *Ann. Rev. Mater. Sci.*, 43:437, 1992.

[73] Y. Xia and G. M. Whitesides. Soft lithography. *Angew. Chem. Int. Ed.*, 37:550–575, 1998.

[74] J. L. Wilbur, A. Kumar, E. Kim, and G. M. Whitesides. Microfabrication by microcontact printing of self-assembled monolayers. *Adv. Mater.*, 6:600–604, 1994.

[75] J. Huang, D. A. Dahlgren, and J. C. Hemminger. Photopatterning of self-assembled alkanethiolate monolayers on gold: a simple monolayer photoresist utilizing aqueous chemistry. *Langmuir*, 10:626–628, 1994.

[76] C. S. Dulcey, J. H. Georger Jr., V. Krauthamer, D. A. Stenger, T. L. Fare, and J. M. Calvert. Deep uv photochemistry of chemisorbed monolayers: patterned coplanar molecular assemblies. *Science*, 252:551–554, 1991.

[77] G. Gillen, S. Wight, J. Bennett, and M. J. Tarlov. Patterning of self-assembled alkanethiol monolayers on silver by microfocus ion and electron beam bombardment. *Appl. Phys. Lett.*, 65(5):534–536, 1994.

[78] N. L. Abbott, J. P. Folkers, and G. M. Whitesides. Manipulation of the wettability of surfaces on the 0.1 to 1 micrometer scale through micromaching and molecular self-assembly. *Science*, 257:1380–1382, 1992.

[79] G. P. Lopez, H. A. Biebuyck, C. D. Frisbie, and G. M. Whitesides. Imaging of features on surface by condensation figures. *Science*, 260:647–649, 1993.

[80] S. Jiang. Molecular simulation studies of self-assembled monolayers of alkanethiols on au(111). *Molecular Physics*, 100(14):2261, 2002.

[81] H. Gronbeck, A. Curioni, and W. Andreoni. Thiols and disulfides on the au(111) surface: the headgroup-gold interaction. *J. Am. Chem. Soc.*, 122(16):3839, 2000.

[82] H. Sellers, A. Ulman, Y. Shnidman, and J. E. Eilers. Structure and binding of alkanethiolates on gold and silver surfaces - implications for self-assembled monolayers. *J. Am. Chem. Soc.*, 115(21):9389, 1993.

[83] J. Yang, J. Han, K. Isaacson, and D. Y. Kwok. Effects of surface defects, polycrystallinity, and nanostructure of self-assembled monolayers for octadecanethiol adsorbed onto au on wetting and its surface energetic interpretation. *Langmuir*, 19:9231–9238, 2003.

[84] K. K. Berggren, A. Bard, J. L. Wilbur, J. D. Gillaspy, A. G. Helg, J. J. McClelland, S. L. Rolston, W. D. Phillips, M. Prentiss, and G. M. Whitesides. Microlithography by using neutral metastable atoms and self-assembled monolayers. *Science*, 269:1254–1257, 1995.

[85] M. L. Chabinyc, J. C. Love, J. H. Thywissen, F. Cervelli, M. G. Prentiss, and G. M. Whitesides. Self-assembled monolayers exposed to metastable argon beams undergo thiol exchange reaction. *Langmuir*, 19:2201–2205, 2003.

[86] H. Ozaki and Y. Harada. Penning ionization electron spectroscopy of n-alkane ultrathin films. molecular orbitals and orientation of molecules. *J. Am. Chem. Rev.*, 112:5735–5740, 1990.

[87] H. Seiler. Secondary electron emission in the scanning electron microscope. *J. Appl. Phys.*, 54(11):R1–R18, 1983.

[88] M. Argument, Y. Y. Tsui, R. Fedosejevs, J. Li, and P. Herman. Drilling and micromachining of glasses with uv and vuv laser pulses. *Photons*, 1(2):15–17, 2004.

[89] F. Sauli. Gem: a new concept for electron amplification in gas detectors. *Nucl. Instr. and Meth. A*, 386:531–534, 1997.